Deformation of Cohesionless Fill Due to Cyclic Loading

SPR ID# C-05-03

FINAL REPORT
October, 2007

Submitted by

Sophia Hassiotis, Associate Professor
Kai Xiong, Research Assistant

Department of Civil, Environmental and Ocean Engineering
Stevens Institute of Technology
Hoboken, N.J. 07030

The 2005 UTRC Research Initiative
Region II

In cooperation with

New York State Department of Transportation
and
U.S. Department of Transportation

Disclaimer Statement

“The contents of this report reflect the views of the author(s) who is (are) responsible for the facts and the accuracy of the data presented herein. The contents do not necessarily reflect the official views or policies of the UTRC, NYSDOT, NJDOT or the Federal Highway Administration. This report does not constitute a standard, specification or regulation.”

The contents of this report reflect the views of the authors, who are responsible for the facts and the accuracy of the information presented herein. This document is disseminated under the sponsorship of the Department of Transportation, University Transportation Centers Program, in the interest of information exchange. The U.S. Government assumes no liability for the contents or use thereof.

TECHNICAL REPORT STANDARD TITLE PAGE

1. Report No.	2.Government Accession No.	3. Recipient's Catalog No.

4. Title and Subtitle	5. Report Date
Deformation of Cohesionless Fill Due to Cyclic Loading	October 2007
	6. Performing Organization Code SPR ID# C-05-03
7. Author(s) Sophia Hassiotis, Kai Xiong	8. Performing Organization Report No.
9. Performing Organization Name and Address Stevens Institute of Technology Castle Point on Hudson Hoboken, N.J. 07030	10. Work Unit No. 11. Contract or Grant No.
12. Sponsoring Agency Name and Address Federal Highway Administration, U.S. Department of Transportation, Washington, D.C. New York State Department of Transportation, Albany, NY University Transportation Research Center, City College of New York New York, NY 10031	13. Type of Report and Period Covered Final Report –SPR ID#C-05-03 14. Sponsoring Agency Code
15. Supplementary Notes	

16. Abstract

EXECUTIVE SUMMARY

Integral abutment bridges are becoming widely accepted for new construction of short to medium length highway bridges of limited skew. Although they offer an economic alternative to the use of bearings, integral abutments present their own unique challenges. One area of concern is the development of passive pressures behind the abutment due to the cyclic loading of the soil during thermal movement of the superstructure. The challenge of the present work is to present to the engineering community the best estimate of the passive pressures behind the abutment.

To meet the challenge, we review both, the classic earth pressure theories and the more recent displacement-dependent theories used to describe the development of passive pressures. The information is compared to 1) the soil-pressure data obtained from the Scotch-Road Integral Abutment Bridge that was instrumented by the Stevens Institute of Technology; 2) additional data on two full-scale tests that were obtained from the literature; and 3) data from laboratory tests found in literature.

Finally, we suggest two K_p factors that should be used for the calculation of passive pressures behind a cyclically moving abutment. For relatively short bridges, the NCHRP curve for dense sand can be used. For longer bridges that experience large enough displacements to guarantee the applicability of the classic earth pressure theories, a Rankine pressure for dense sands was found adequate. For either case, a linear distribution of pressure is suggested.

17. Key Words	18. Distribution Statement
Integral Abutments, Bridge Testing, Passive Pressure	No Restriction

19. Security Classif (of this report)	20. Security Classif. (of this page)	21. No of Pages	22. Price
Unclassified	Unclassified	82	NA

Form DOT F 1700.7 (8-69)

Acknowledgement

This research was funded by the U.S. DOT University Transportation Centers Program and the Research Foundation of the City University of New York. Matching funding was provided by the Stevens Institute of Technology and the NJDOT. The authors would like to thank Dr. Camille Kamga and Dr. James Baker for their support.

TABLE OF CONTENTS

LIST OF FIGURES

LIST OF TABLES

CHAPTER 1- INTRODUCTION

What is an Integral Abutment Bridge (IAB)

Traditionally, the bridge superstructure is connected with the substructure with expansion joints, which accommodate the superstructure's deformation due to the daily and seasonal thermal variations. Figure 1 shows a typical design of a traditional bridge, where bearings are used at the connection of the bridge to the abutment. In contrast, integral bridges are connected monolithically with the abutment with a moment-resisting connection as shown in Figure 2.

Advantages of Integral Abutment Bridges

The main advantage of an integral abutment bridge is in the elimination of the problems associated with the use of joints and bearings. The integral structures can eliminate joint-related damage caused by the use of deicing chemicals and restrained growth of rigid movement, thus reducing long-term maintenance costs. Integral bridges are regarded as best choices, particularly in cold climate-areas such as the northern United States, Canada and northern Europe. [1]

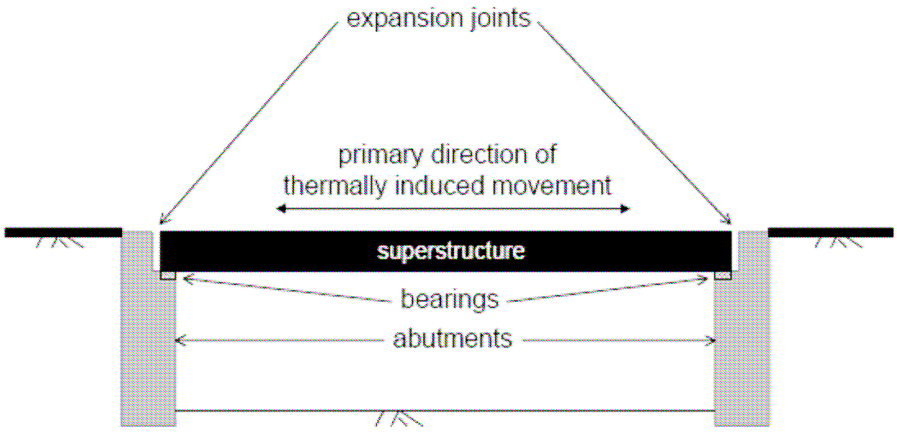

Figure 1. Conventional bridge design [2]

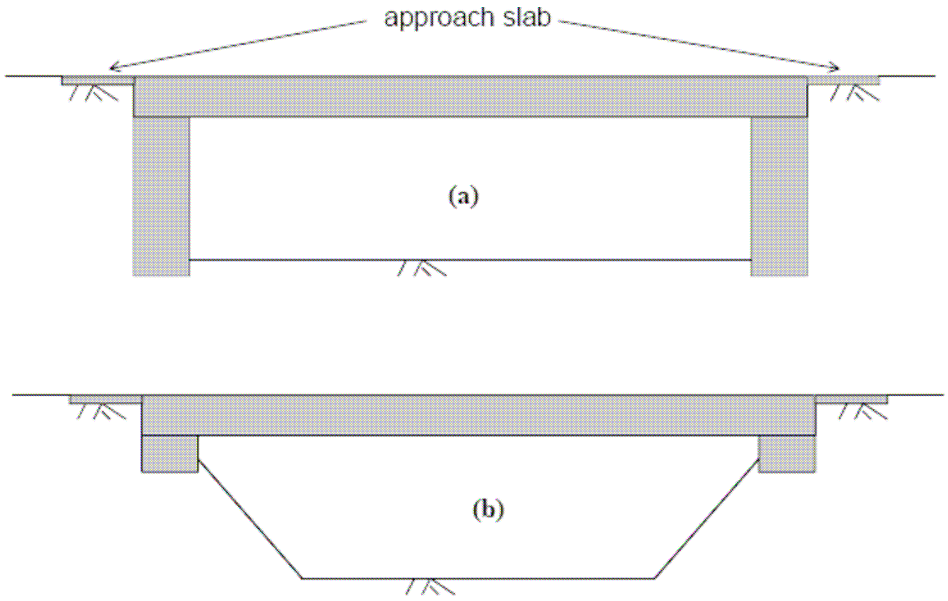

Figure 2. Integral abutment bridge design [2]

Some of the advantages of integral abutment bridges are summarized in [3] as:

- Reduced initial cost and long-term maintenance.
- Elimination of deck joints.
- Elimination of bearings, anchor bolts, grouting etc.
- Elimination of leakage onto critical structural elements.
- Reduced number of foundation piles.
- Elimination of potential for tilting piers.
- Increased reserve load capacity and load distribution, resulting in more resistance to damaging effects of overloads.
- In-built resistance to uplift at abutment end.

Problems and uncertainties of integral Abutment Bridge

Although integral abutment bridges have many advantages compared with the traditional bridges, some problems and uncertainties still remain and are summarized as follows in [4]:

- Temperature-induced movements of the abutment cause settlement of the approach fill, resulting in a void near the abutment if the bridge has approach slabs. Traffic loads also contribute to approach fill settlement.

- Secondary forces can cause cracks in concrete bridge abutments. Wing-walls can crack due to rotation and contraction of the superstructure.
- Skewed integral bridges tend to rotate under the influence of cyclic changes in earth pressures on the abutment.
- Bridge abutments can be undermined due to water entering into the approach fills at the bridge ends.
- The piles that support the abutments may be subjected to high stresses as a result of cyclic expansion and contraction of the bridge superstructure. These stresses can cause formation of plastic hinges in the piles, and may reduce their axial load capacities.
- Integral bridges cannot be used with weak embankments or subsoil, and they can only be used for limited lengths, although the maximum length is still somewhat unclear. Integral bridges are suitable if the expected temperature-induced movement at each abutment is 0.051m (2 in.) or less, and somewhat larger movements may be tolerable.

A full survey of current issues on the use of integral abutment is found in [5].

Objectives and organization of research

The objective of this report is to present the abutment deformation and soil pressure data behind integral bridges, study the pressure distribution in light of classical and later work on the development of such pressures, and share pertinent findings with the research and design community.

Chapter 2 is the review of some classic earth pressure theories. Chapter 3 introduces relevant laboratory experiments found in literature. Chapter 4 summarizes the findings of several full-scale tests. Chapter 5 describes the full-scale testing of the Scotch Road Bridge in Trenton, N.J., and the comparison of the recorded data with the existing theories. Chapter 6 contains the summary of this research, and the conclusions and recommendations about the pressure magnitude and distribution behind the abutment of an IAB.

CHAPTER 2- LITERATURE REVIEW OF EARTH PRESSURE THEORIES

Overview

Conventionally, Coulomb or Rankine theories have been used for the design of retaining structures because of their simplicity.[6] In the evaluation of pressures behind integral abutments, most transportation departments of United States design for passive pressures.[7] At least two agencies neglect soil pressure in smaller bridges and three agencies neglect earth pressure in all their designs.[7] In most cases, researchers have advocated the use of a Rankine passive pressure magnitude and distribution.[8] However, classic earth pressure theories are based on a planar failure surface assumption, which is hard to achieve in real situations. In addition, a comparison of the passive earth pressure coefficient K_p calculated with theories proposed by Caquot and Kerisel, Brinch-Hansen, Janbu, Sokolovski, and Terzaghi and Peck concluded that the classical theories overestimate passive resistance. (See references 9, 10, 11, 12, 13, and 14)

A pressure envelope that combines a passive pressure envelope using Rankine passive pressure coefficients K_p in the upper third of the wall and Rankine active pressure coefficients K_a towards the base of the abutment has been proposed in the past to be used for design of integral abutments.[15] This method is based on the premise that higher lateral earth pressures develop at the top of the wall, and less pressures at the bottom as the movement of the wall subsides at its base. Approximate methods for estimating the displacement-dependent earth pressures have also been developed by other researchers and can be used in the case of integral abutments. (See references 16, 17, 18, and 19)

In the design of the superstructure itself, some researchers recommend that only two thirds of the full passive pressures be used for most integral bridges.[20, 21] Since the bending moments induced by passive pressures on abutments counteract the dead and live load bending moments in simple spans, bridge designers should adopt a conservative approach regarding earth pressures on abutments when designing the superstructure. For example, if the designer

chooses to account for the earth pressures, overestimating their value would lead to nonconservative bending moments in spans. (4)

Planar Failure Surface Earth pressure theories

The classical theories of Coulomb and Rankine can be used to calculate the minimum active and maximum passive pressures. These theories are based on the assumption of a linear plane failure surface. Usually, the assumption of plane failure surfaces gives reasonable estimates of the active earth pressure but overestimates the passive pressure.

Rankine's Theory

Rankine's theory assumes a linear variation of stress along a depth z of a frictionless wall with horizontal backfill as:

$$\sigma_a = K_a \gamma z \qquad (1)$$

$$\sigma_p = K_p \gamma z \qquad (2)$$

in which K_a and K_p ,the active and passive earth pressure coefficients respectively, are defined as:

$$K_a = \cos\beta \left[\frac{\cos\beta - \left[\cos^2\beta - \cos^2\phi\right]^{1/2}}{\cos\beta + \left[\cos^2\beta - \cos^2\phi\right]^{1/2}} \right] \qquad (3)$$

$$K_p = \cos\beta \left[\frac{\cos\beta + \left[\cos^2\beta - \cos^2\phi\right]^{1/2}}{\cos\beta - \left[\cos^2\beta - \cos^2\phi\right]^{1/2}} \right] \qquad (4)$$

Here, β is the inclination of the embankment, and φ is the angle of internal friction. If the embankment is level (β =0) the equations are simplified as follows:

$$K_a = \frac{1-\sin\phi}{1+\sin\phi} = \tan^2(45^0 - \frac{\phi}{2}) \qquad (5)$$

$$K_p = \frac{1+\sin\phi}{1-\sin\phi} = \tan^2(45^0 + \frac{\phi}{2}) \qquad (6)$$

The Rankine formula for passive pressure can only be used correctly when β is zero or negative. If a large wall friction value can develop, Rankine's theory is not correct and will give less conservative results. Rankine's theory is not intended to

be used for determining earth pressures directly against a wall (a friction angle does not appear in the equations above). The theory is intended to be used for determining earth pressures on a vertical plane within a mass of soil.

Coulomb's Theory

More than 200 years ago, Coulomb presented a theory for active and passive earth pressures against retaining walls. Generally, he is considered to be the first scientist to develop a theory to predict the passive earth pressure coefficient. In his theory, Coulomb also assumed that the failure surface is a plane. Different from Rankine's theory, Coulomb uses the wall friction, δ, to reduce the active and passive earth pressure coefficients:

$$K_a = \frac{\cos^2 \phi}{\cos \delta [1 + \{\sin(\delta + \phi) \sin \phi / \cos \delta\}^{1/2}]^2} \qquad (7)$$

and

$$K_p = \frac{\cos^2 \phi}{\cos \delta [1 - \{\sin(\phi - \delta) \sin \phi / \cos \delta\}^{1/2}]^2} \qquad (8)$$

For zero wall friction, these reduce to the Rankine coefficients. For granular material, δ is in the range of $\phi/2 < \delta < 2/3\phi$. [22]

Non-Planar Failure Surface Earth pressure theories

The assumption of plane failure surfaces gives reasonable estimates of the active earth pressure but overestimates the passive pressure. Theories based on curved failure theories have been accepted as producing more accurate passive pressures.

Log-spiral Theory

Terzaghi[14] described a theory based on a failure surface in the shape of a log-spiral. The logarithmic spiral earth pressure theory provides more accurate estimates of passive pressures for conditions where the interface friction angle δ is more than about 40% of the angle of internal friction.[23] It compares well with alternative theoretical procedures, for a wide range of values of δ and φ. For

example, numerical analyses based on plasticity theory are in close agreement with this theory.(See references 24, 25, 26, and 27)

The theoretical failure surface during passive pressure consists of two zones: 1) the Prandtl zone, which is bounded by a logarithmic spiral, and 2) the Rankine zone, which is bounded by a plane, as shown in Figure 3. The shape of the log spiral failure surface is shown in Figure 4. The theory is based on the principle that force vectors acting on the log spiral failure surface make angles of φ with the tangent to the spiral, and the lines of action of the force vectors pass through the center of the spiral.

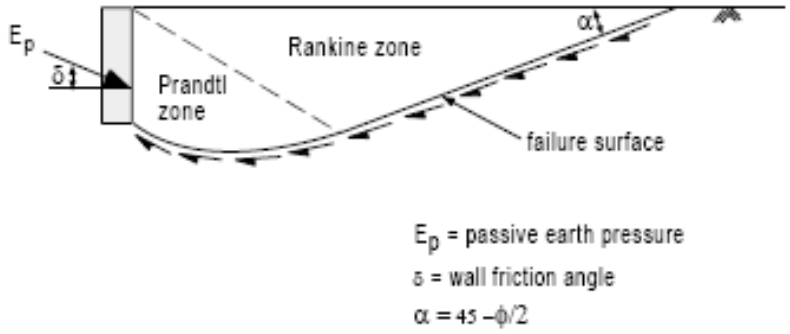

Figure 3. Theoretical shape of passive failure zone(28)

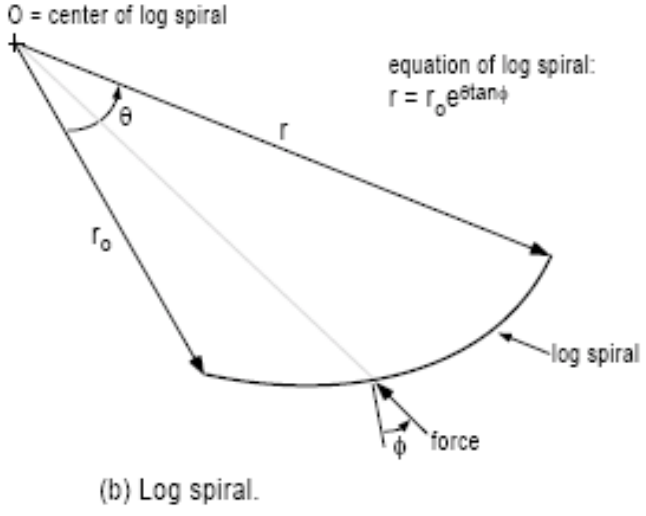

Figure 4. Log-Spiral theory failure mechanism(28)

Slip-Line Field Theory

Sokolovoski[13] introduced a theory termed the 'Slip-Line Field Theory'. In this analysis, it is assumed that failure occurs at constant volumes of soil along slip lines that meet the Mohr-Coulomb failure criterion. This method has the advantage of providing a statistically admissible stress state that satisfy the following equations of equilibrium involving the normal, σ, and shear, τ stresses:

$$\frac{\partial \sigma_x}{\partial x} + \frac{\partial \tau_{yx}}{\partial y} = \gamma$$
$$\frac{\partial \tau_{xy}}{\partial x} + \frac{\partial \sigma_y}{\partial y} = 0 \qquad (9)$$
$$\tau_{xy} = \tau_{yx}$$

The Mohr-Coulomb criteria states that at yield the following formula must apply everywhere in the sand mass:

$$\left(\sigma_x - \sigma_y\right)^2 + 4\tau_{xy}{}^2 = \left(\sigma_x + \sigma_y\right)^2 \sin^2 \phi \qquad (10)$$

The solution of these equations is called Kotter's Equation and gives the orientation of the slip lines together with the stresses on the failure surface. Sokolovoski accomplished the solution through the use of numerical integration.[29]

Method of Slices

In this method, the sliding body is divided up into slices. The individual slices satisfy equilibrium but equilibrium is not necessarily satisfied over the entire sliding body as a whole.

Several researchers have advanced this method. In one, a circular failure surface is assumed and equilibrium of vertical force and moment is satisfied.[30] The method was made more accessible by creating charts of K_p versus ϕ,[12] and it was further refined by making an assumption a log-spiral failure surface, coupled with a straight-line portion (see Figure 5) [31]. All methods rely on the

questionable assumption that the factor of safety is the same for all points of the sliding surface.

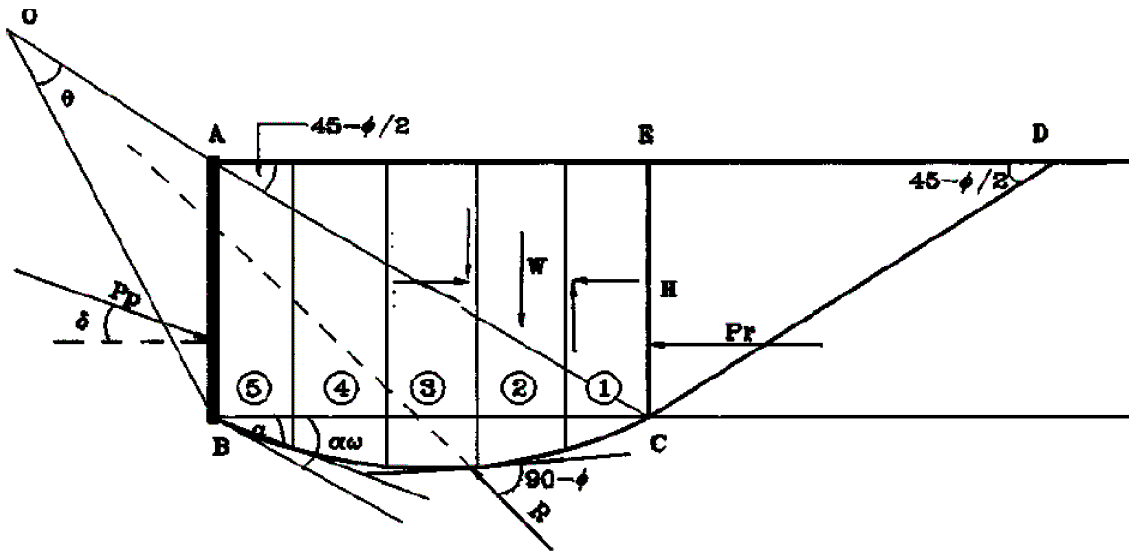

Figure 5. Failure surface of 'method of slices' [31]

Displacement-dependent Earth pressure theories

Non-planar surface assumptions give good results in the prediction of the earth pressure, but they still lack of accuracy. Recently, engineers and researchers have attempted to relate the development of earth pressure to the wall displacement. Researchers have produced values for the lateral wall movements needed to create active and passive pressures.[17] For sand, these are reproduced in Table 1. Here, Δ is the horizontal displacement at the top of the wall due to rotation or translation and H is the height of the wall. The assumption is of a rigid wall.

Table 1 -Approximate displacement to achieve minimum active or maximum passive pressures in sand [17]

Backfill	Δ/H	
	Active	Passive
Dense Sand	0.001	0.01
Medium Sand	0.002	0.02
Loose Sand	0.004	0.04

In presence of flexible walls, the problem becomes more complicated. Although the assumption for integral abutment design is that the abutment is rigid, this is not the case. Data and finite element analyses has shown that the abutment transmits only part of the bridge displacement to the piles supporting the abutment, pointing to a flexible behavior of the abutment.[32] This, coupled by the fact that the pressure behind an integral abutment is developing during daily and seasonal cyclic loading, creates a pressure distribution behind the abutment that is difficult to predict. It was not until recently that experimental work and modeling concentrated in defining the mechanics of the soil behind an integral abutment.

For the design of integral abutments, the displacement Δ at the top of the abutment is found by assuming that the total bridge displacement is divided equally between each abutment:

$$\Delta = 1/2 L \alpha \Delta T \qquad (11)$$

where *L* is the length of the continuous bridge; *α* is the coefficient of thermal expansion; *ΔT is* the difference between the temperature during construction and the maximum (or minimum) temperature expected at the site (See Figure 6).

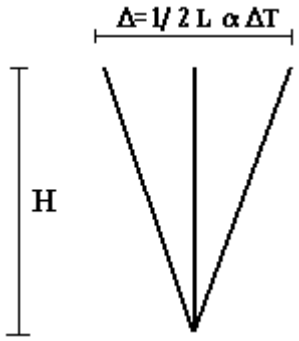

Figure 6. Definition of wall-top displacement

For consistency in notation in this report, K_p will henceforth refer to a maximum attainable coefficient of earth pressure, while K_h will refer to an intermediate coefficient of earth pressure that depends on wall movement.

Three equations that can be used to produce K_h as a function of wall movement are summarized below. The research that yielded these equations is summarized in detail in the chapters that follow.

Massachusetts Bridge Manual

In the design of integral abutments, Massachusetts uses a magnitude of lateral earth pressure that depends on the movement of the abutment. The value is assumed to be somewhere between at-rest conditions and passive pressures. Used with the Mass Highway's standard compacted gravel borrow, a pressure coefficient K_h is proposed as:[33]

$$K_h = 0.43 + 5.7[1 - e^{-190(\Delta / H)}] \qquad (12)$$

where, Δ is displacement of the abutment and H is the height of the abutment. The pressure varies linearly at the back of the abutment.

British Code 42 for Passive Coefficient

The British Code BA42 proposes an upper limit of the passive coefficient as

$$K_h = (\frac{\Delta}{0.05H})^{0.4} K_p \qquad (13)$$

where a maximum value for K_p, derived after cyclic loading of Leighton Buzzard sand, is taken to be 12.5. The minimum K_h is constrained to $K_p/3$.
The pressure distribution in this code is linear down to H/2 and constant to H.

Passive Coefficient as a refinement to the British Code 42

Researchers in England proposed the same pressure distribution with BA42 and a new equation for the passive pressure coefficient as:

$$K_h = K_o + (\frac{\Delta}{0.03H})^{0.6} K_p \qquad (14)$$

where the constrain for the minimum K_h is removed.[19] The work is based on testing of a model rigid wall that was used to study the effects of thermal loading on integral abutments. The model simulated an abutment, which was free to rotate about its base as a response to cyclic loading of the top. As such this coefficient may not be directly applicable to an integral abutment supported on piles. Such abutments experience translation as well as rotation. However, the

tests give a good understanding about the built-up of lateral soil stresses that result from the induced cyclic loading.

Figure 7 compares the passive pressure coefficients expected by a given wall displacement by 1) the Massachusetts Bridge Manual, 2) the British Code 42 and 3) England et al. [19] Such theories were developed with the help of laboratory or large-scale testing, and will be analyzed in detail in the next sections.

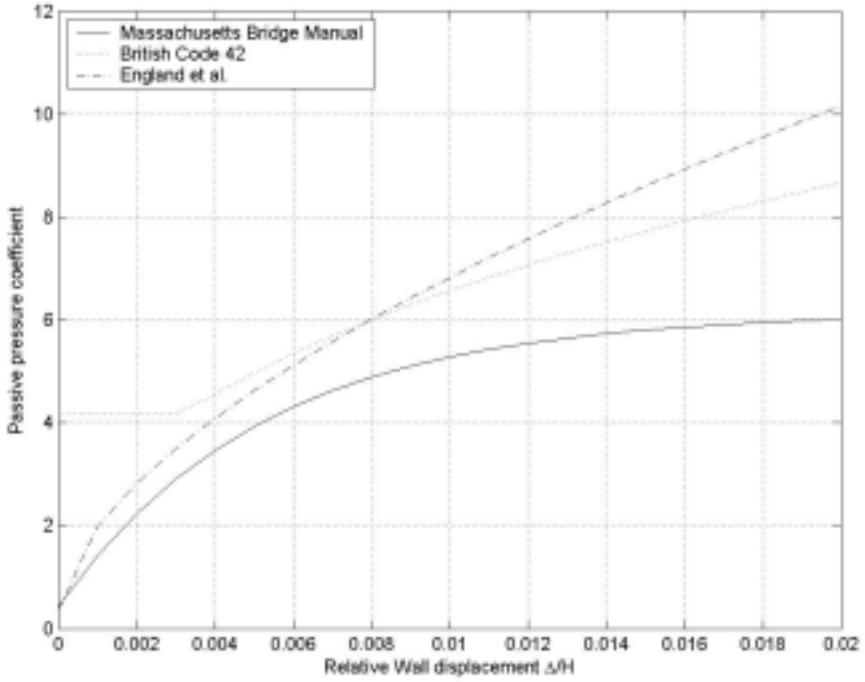

Figure 7. Displacement-dependent K_h-curves

CHAPTER 3- A REVIEW OF LABORATORY TESTS ON DEVELOPMENT OF LATERAL PRESSURE

Many integral abutment bridges have been built in North America, Canada, and Europe in recent years due to the simplicity of design and the reduced maintenance cost. The abutments of the bridge are designed to sustain the lateral earth pressure in addition to the vertical pressures. For integral abutment bridges, there are some uncertainties in calculating the distribution and magnitude of the lateral earth pressure, due to the existence of cyclic motion on the system. In general, the soil pressure is a function of the type of soil, the soil unit weight γ, the friction angle Φ, the degree of compaction, the location of the ground-water table, the magnitude and location of surcharge loads and, to a greater extent, the degree of displacement and rotation of the retaining structure.

Researchers have developed experiments to shed light to the mechanism responsible for the complexity of the lateral earth pressure behind the cyclically moving integral abutment. Generally, there are two major research avenues, one based on laboratory experiments, and another on full-scale measurements of bridge behavior. In this section, some experimental setups and relevant findings will be described.

Passive earth pressures at various wall movements

In the early 1990's researchers conducted an experiment to study the development of earth pressure against a vertical rigid wall, and studied the effect of both, the magnitude and the mode of deformation on the pressure magnitude and distribution.[34]

Two categories of wall movement were studied: rotation about a point above the top (RTT), and rotation about a point below the wall base (RBT), as shown in Figure 8 (a) and (b) respectively. A parameter n is employed to indicate the mode of deformation. In either of these two categories of wall movement, a value for n of zero represents pure rotation, and a value of infinity represents pure translation.

In general, for the translation mode, it was found that Rankine's theory, which doesn't consider the wall friction effect, underestimates the passive pressure, while Coulomb's theory, which takes into account the effect of the wall friction, overestimates the passive pressure. The experimental earth pressure coefficient K_p values fit Terzaghi's prediction based on the general wedge theory very well (as shown in Figure 9 and Figure 10).

For the study of the "RBT" mode, n was varied from 0 to 13.78 and the influence of the resulting wall displacement on the horizontal earth-pressure coefficient, K_h, is shown in Figure 11. For a ratio of a horizontal displacement to wall height, S_{max}/H, of 0.2, K_h continues to increase approaching the Coulomb coefficient of passive pressure.

Figure 12 to Figure15 show the pressure distribution behind the rigid wall for four different n values. Due to the presence of strong rotation, the pressure distribution along the wall is nonlinear. But when n reaches 13.78, the effect of rotation diminishes, and the distribution of earth pressure can be taken as linear.

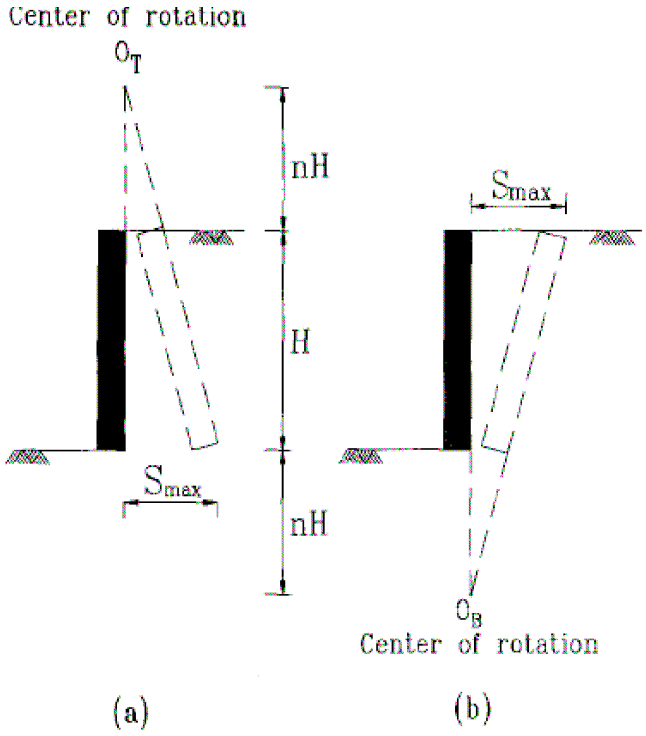

Figure 8. Two types of passive wall movements:
(a) RTT mode; (b) RBT mode [31]

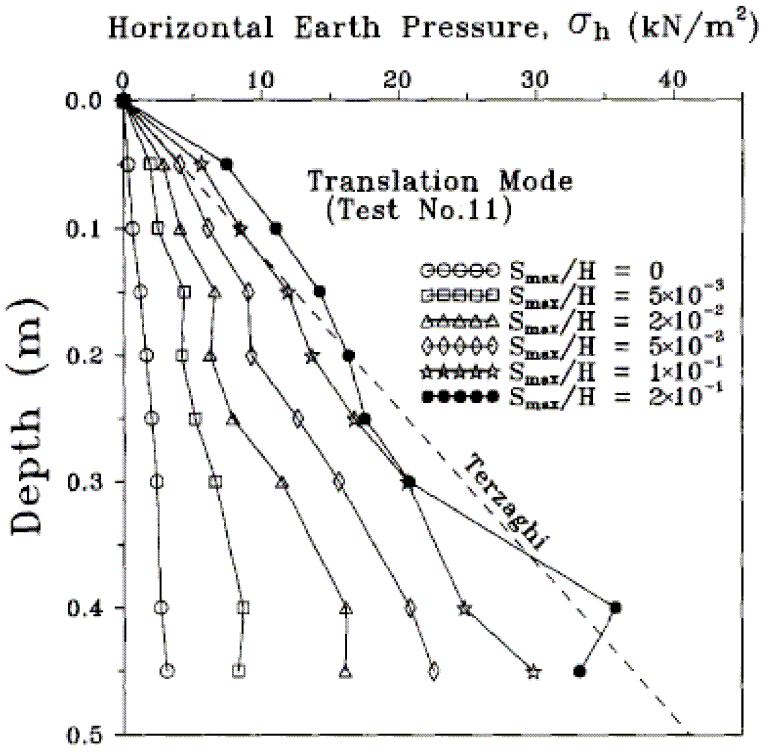

Figure 9. Distribution of horizontal earth pressure for translation mode [31]

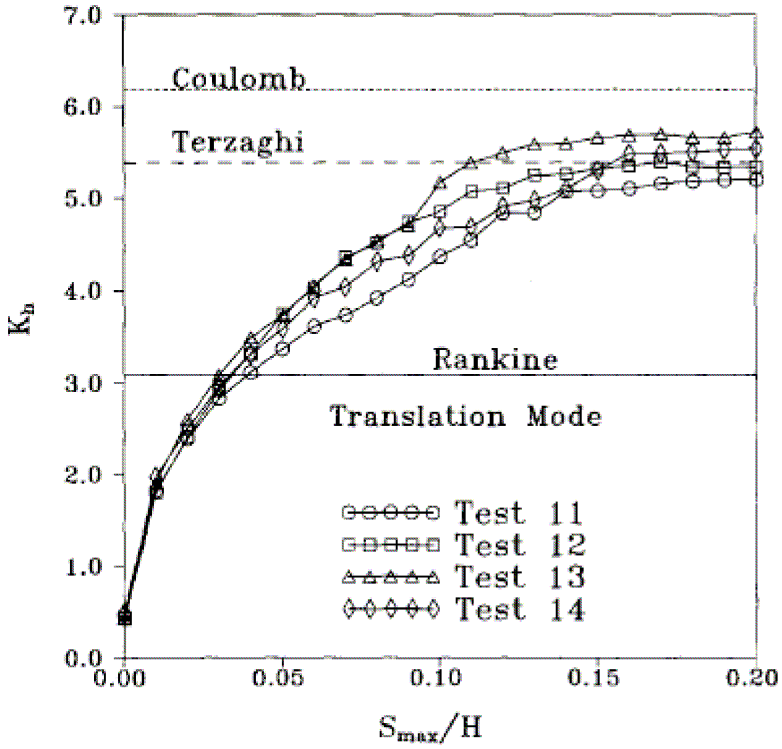

Figure 10.Variation of K_h with relative wall displacement for translation mode[31]

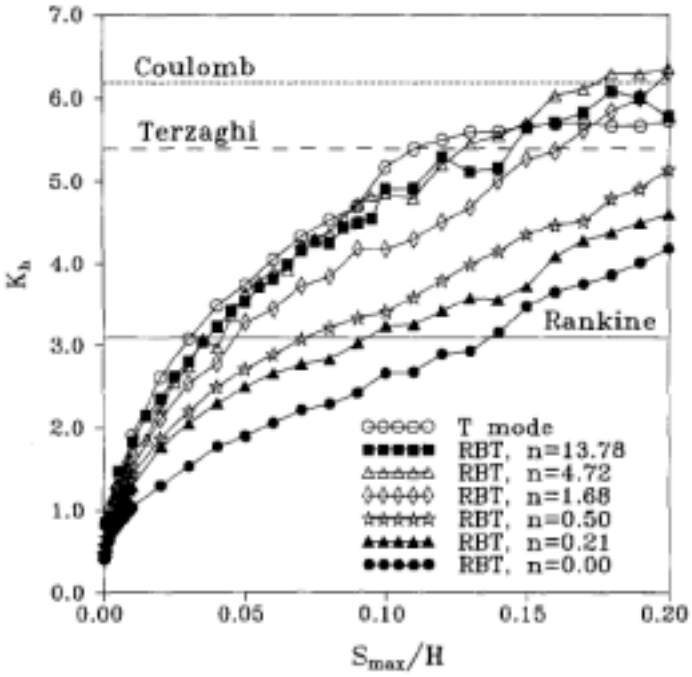

Figure 11. Variation of earth-pressure coefficient K_h with wall movement for RBT mode [31]

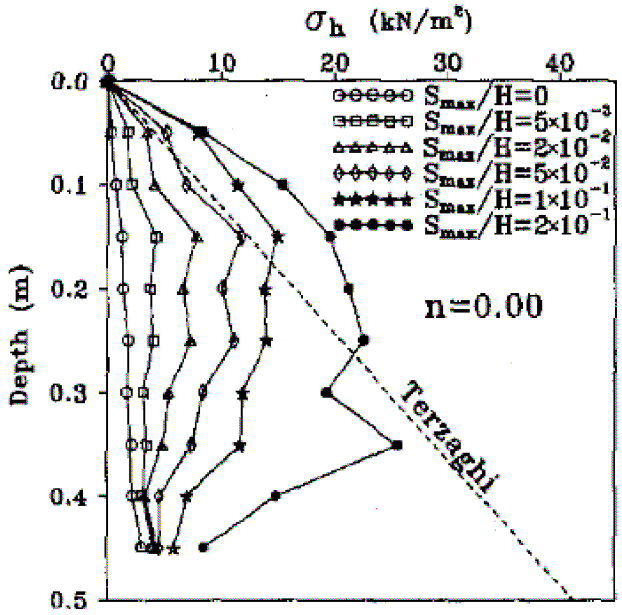

Figure 12. Distribution of horizontal earth pressure for RBT mode for n=0.00 [31]

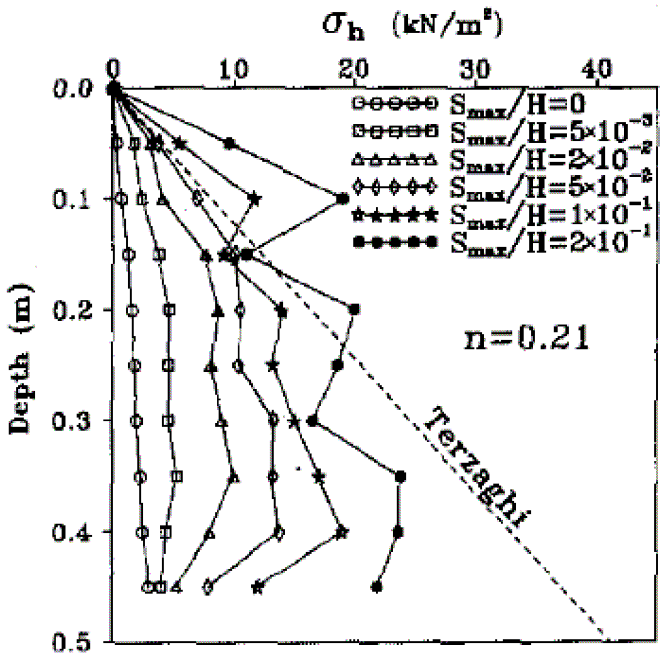

Figure 13. Distribution of horizontal earth pressure for RBT mode for n=0.21 [31]

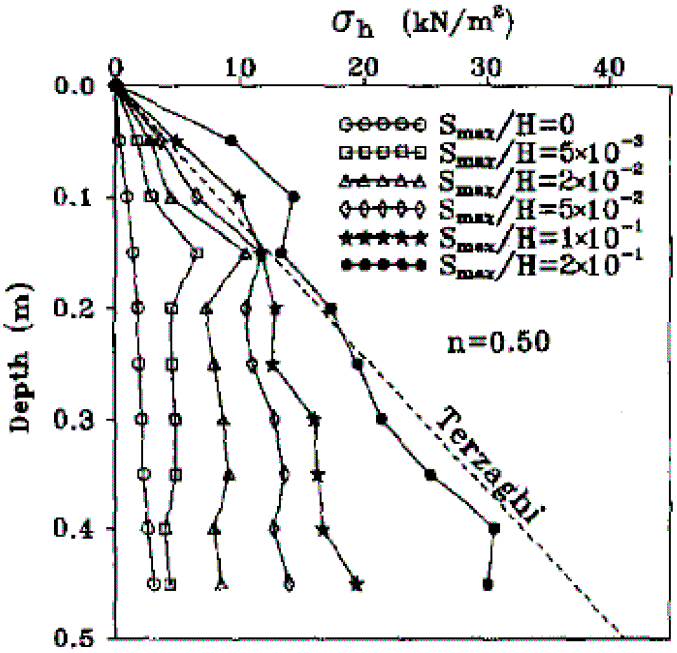

Figure 14. Distribution of horizontal earth pressure for RBT mode for n=0.50 [31]

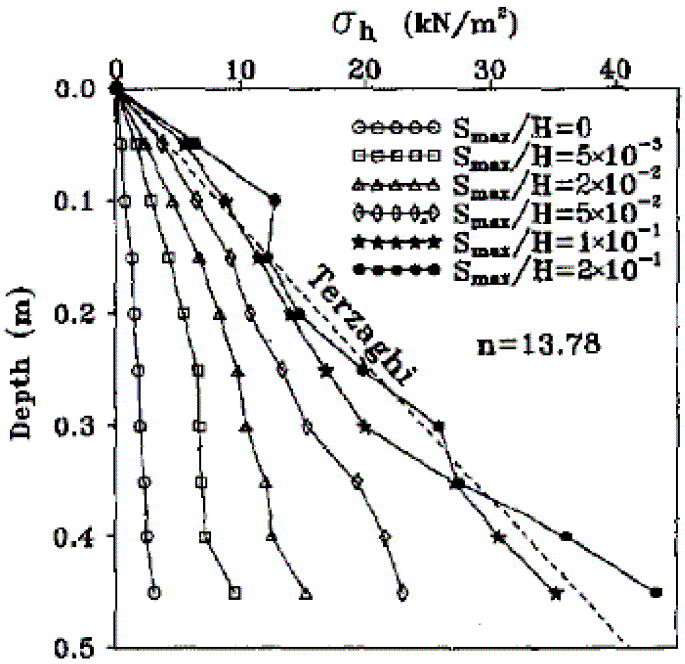

Figure 15. Distribution of horizontal earth pressure for RBT mode for n=13.78 [31]

This study is of interest because in the integral bridges, the integral abutment is connected on the pile tops, which do not fix the rotation. As a result, the wall movements can hardly be defined as pure “translation” or pure “rotation”. It is a combination of these two movement modes. The study presents a good summary of the influence of the wall movement mode and magnitude to the earth pressure. However, it does not consider the effect of cyclic loading on such pressures.

A fundamental approach to the time-temperature loading problem

Experiments indicate that various wall-movement modes have effects on the magnitude and distribution of the earth pressure behind rigid retaining wall. However, few record the effect of the cyclic loading due to the daily and seasonal thermal variation. Such an experiment was conducted recently [19].

An experimental investigation was conducted to study the soil-structure

interaction problem facing integral bridges with full-height abutments. A 1 to 6-scale model-wall was used retaining Leighton Buzzard sand. Seasonal and hourly variation of displacement was imparted in order to determine the manner in which the pressure changes between active and passive wall movements, and also the manner in which the pressure escalates with the number of cycles, leading eventually to a repeating steady state of stress.

Based on the data from the experiments, two major mechanisms were used to explain the pressure magnitude and distribution behind the retaining wall: Granular Flow and Granular Arch. The Flow mechanism relates dominantly to the large wall rotations and the Arch mechanism relates dominantly to small wall rotations. The Flow mechanism allows a continuous uni-directional deformation of the soil mass without cyclic stress variation. The Arch mechanism reduces the vertical stresses acting on the soil behind the lower half of the wall resulting in lower horizontal earth pressures there. [35]

Only the effects of rotation were evaluated since full height integral abutments experience mainly rotational deformation. The results of this study are in agreement with the result for an RBT mode when n equals zero (pure rotation.) For these abutments, the stress distribution can be considered nonlinear. The pressure achieves its maximum value around the middle height of the abutment and decreases towards at the base point of the abutment (as shown in Figure 16).

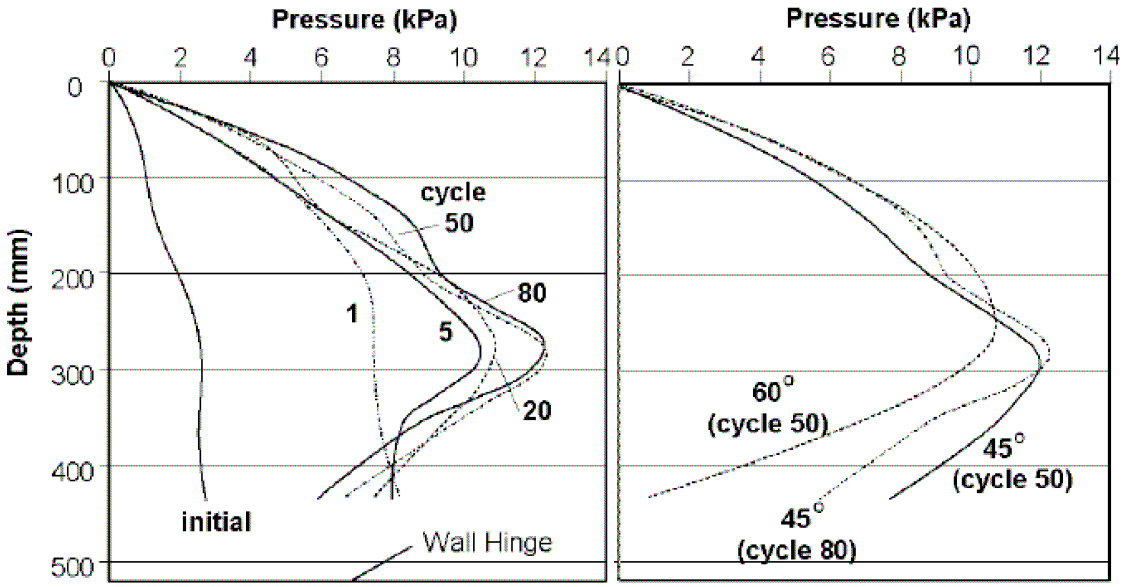

Figure 16. Recorded values of (a) maximum lateral wall pressure for various cycles and (b) average maximum pressure [35]

This experiment sheds light to the deformation of sand due to cyclic loading and to the stress built up due to sand flow, densification and arching. Although the mode of deformation cannot be used to represent an integral abutment on piles, the information can be used to explain pressure built up due to cyclic loading of the integral abutment through daily and seasonal temperature variations. To quote: “During the early cyclic wall rotations, the backfill soil densifies and the soil stress acting on the wall increases. The different ratcheting strain effects close to the wall and away from the wall lead to a continuous flow path which is downwards and away from the wall (close to the wall) and away from the wall and upwards (away from the wall). The resulting effect at the soil surface is settlement close to the wall and possible heave away from the wall.”[19]

Summary

Experiments on passive earth pressures at various wall movements show that the lateral earth pressure coefficient, K_h, increases with wall translation and reaches an upper limit value best predicted by Terzaghi’s general wedge

theory.[34] The pressure distribution behind the retaining wall in pure translation is linear. When combined with a rotational mode of deformation, the pressure distribution is no longer linear, and an upper limit for K_h has not been captured. Studies on the effect of cyclic loading indicate that two mechanisms are responsible for the pressure built up behind integral abutments, granular flow and granular arch. [19,35] The pressure distribution is given as linear down to H/2 and constant to H. The study arrives at best values for the K_h shown in Table 2. This table summarizes the two studies found in this section.

Table 2- Summary of laboratory experiments on passive pressure development

	Effects of Wall movement[34]	Effects of Cyclic Loading[19,35]
Abutment movement modes	Both "Translational" and "Rotational"	Mainly "Rotational"
Loading method	Monotonic	Cyclic
K_h factor proposed	Terzaghi's for "Translational" mode. None given for Rotational mode	$K_h = K_o + (\frac{\Delta}{0.03H})^{0.6} K_p$
Pressure distribution proposed	Linear for "Translational" mode, nonlinear for "Rotation"	Bylinear

CHAPTER 4- A REVIEW OF PRESSURE MEASUREMENT FROM FULL-SCALE INTEGRAL ABUTMENT BRIDGES

Full-scale testing for the Massachusetts Highway Department

The University of Massachusetts, Amherst began a full-scale test in 2002 to evaluate an integral abutment bridge constructed over Millers River in Orange, MA, in the year 2000. The project was sponsored by the Massachusetts Highway Department.

The three-span continuous structure has a total length of 82.3 m (270 ft) and a width of 9.8 m (32.15 ft), as shown in Figure 17.

Figure 18 shows the abutment and approach slab details. The structure includes a 0.2 m (0.656 ft) concrete deck supported on four 1.22 m (4 ft)-deep steel-plate girders that are embedded into the abutment walls.

The researchers recorded the displacement, rotation, and lateral earth pressure for a 4 years period during which the temperature ranged from -23^0C to 37.8^0C. Figure 19 and Figure 20 show the measured and calculated abutment displacements at the centerline-girder at the north and south abutments, respectively. The recorded data show that the displacement of the abutment is a linear function of temperature changes.

Figure 21 presents the seasonal fluctuations of peak soil pressures. At the south abutment, the data show an abrupt increase in pressure during 2004, when compared with the pressure data of 2002. The maximum-recorded earth pressure of the deepest sensor (placed 2.75m (9.05 ft) beneath the top of the south abutment) was measured as 29 ksi (200Mpa) in 2002. This sensor recorded around 43 ksi (296Mpa) by 2004, an increase of approximately 50% in two years.[36]

Figure 22 and Figure 23 show field measured pressure at the south abutment for three different depths during 2002 and 2004 overlaid with the modified NCHRP soil-springs curve. The modified NCHRP curves appear to fit much of the data.[37]

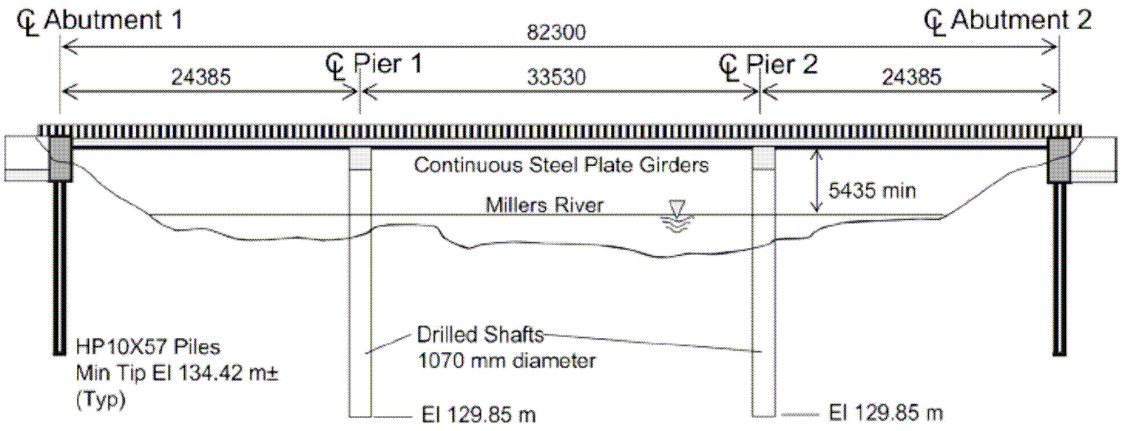

Figure 17. Side view schematic of Orange-Wendell Bridge [36]

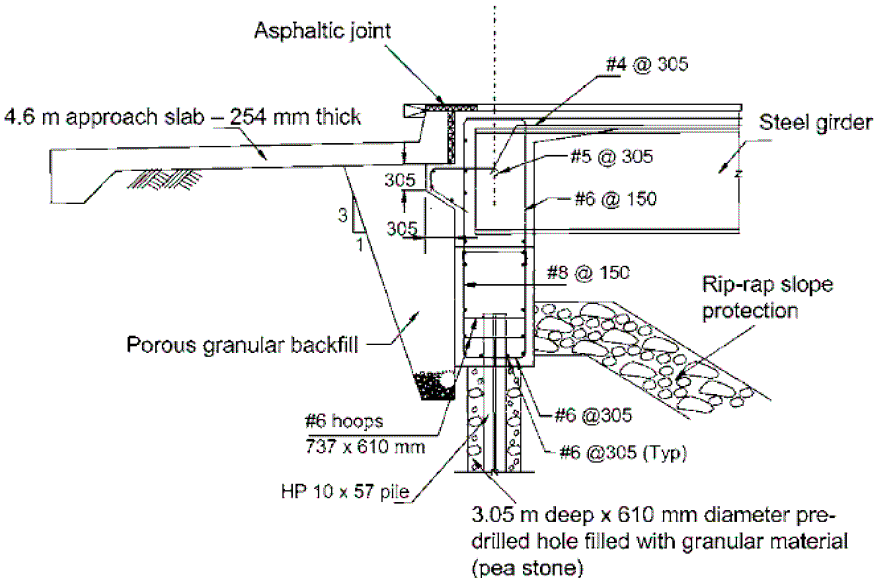

Figure 18. Abutment and approach slab details [36]

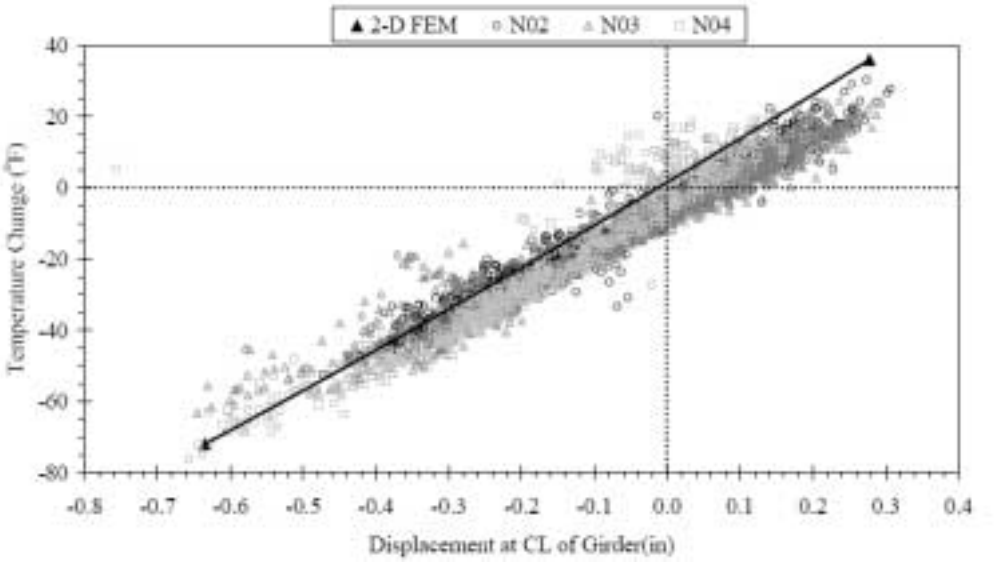

Figure 19. Measured and calculated North abutment displacement at centerline of girder [36]

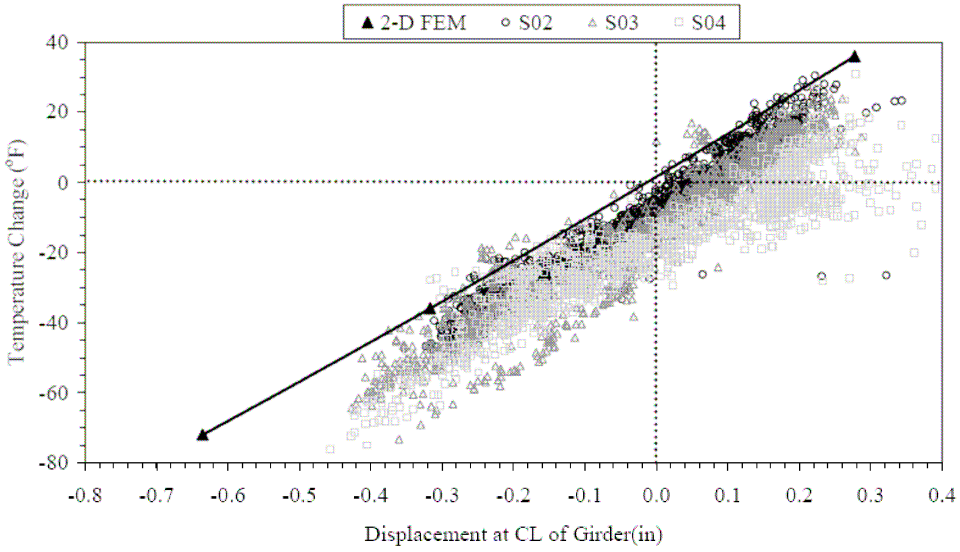

Figure 20. Measured and calculated South abutment displacement at Centerline of Girder [36]

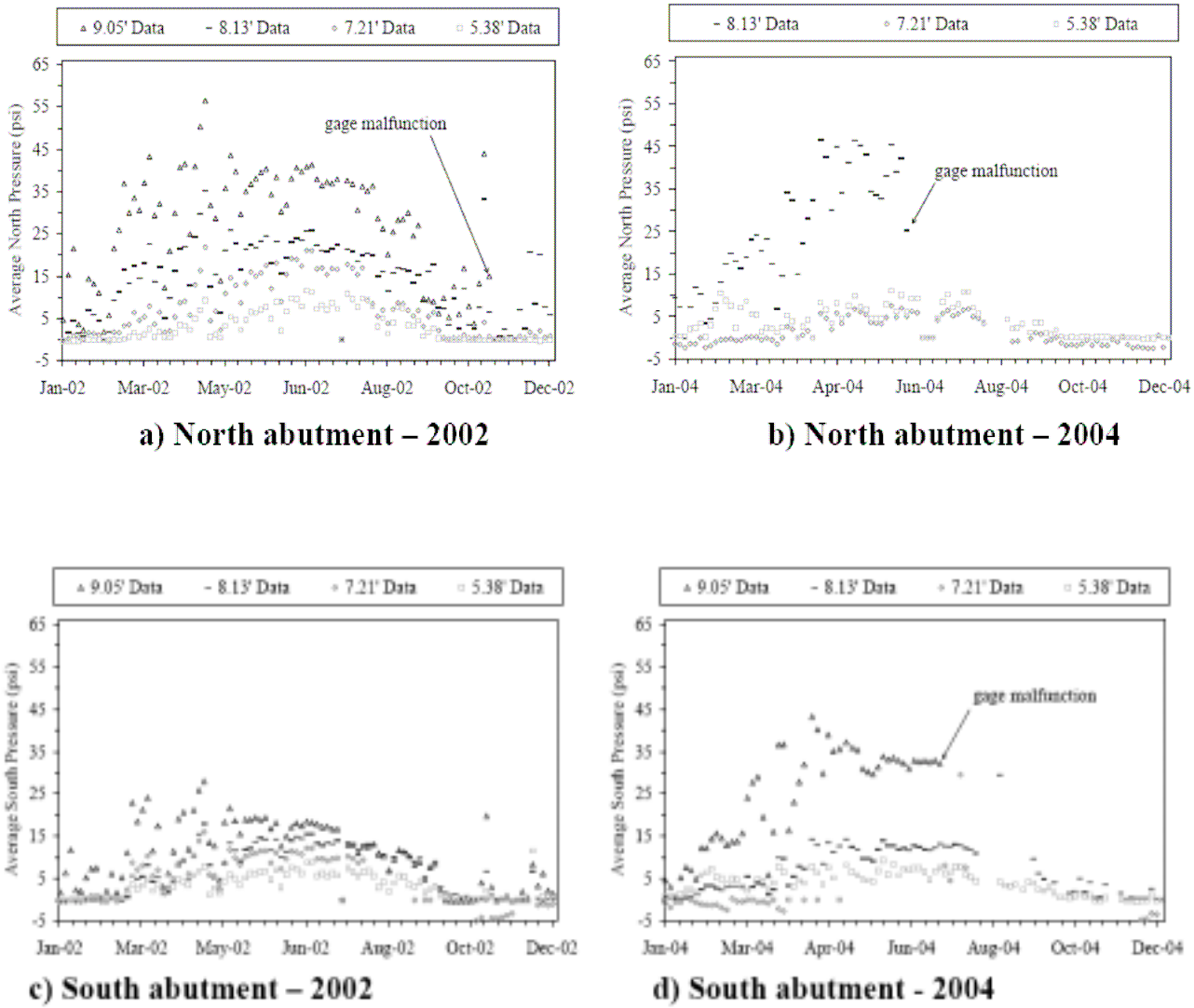

Figure 21. Seasonal Fluctuations of Peak Soil Pressures [36]

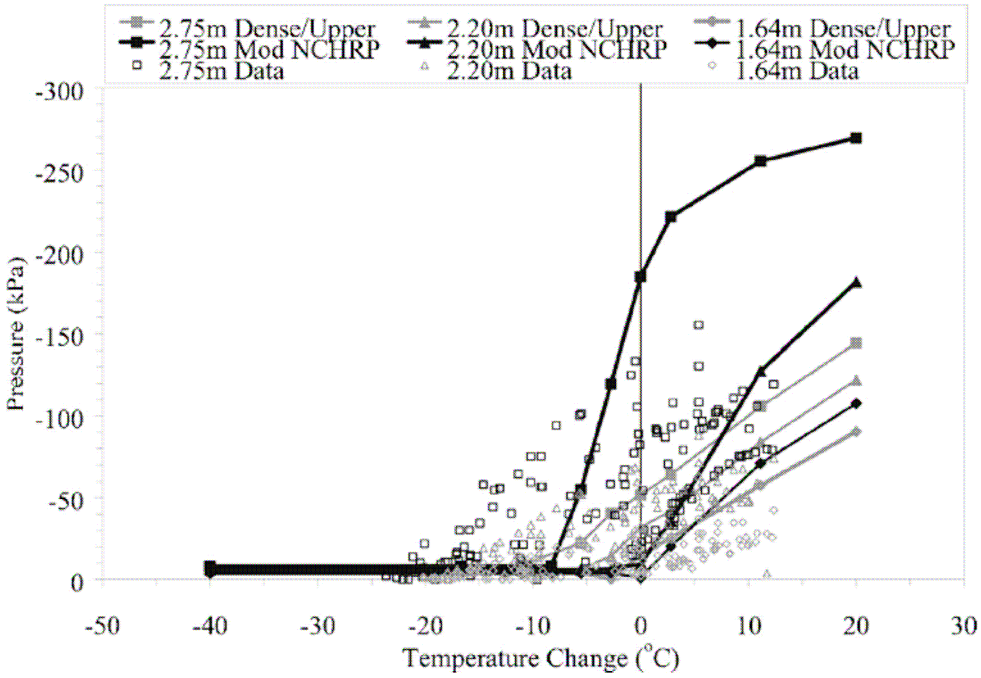

Figure 22. Average earth pressure at south abutment vs temp. change, 2002 [37]
*1m=3.2808 ft

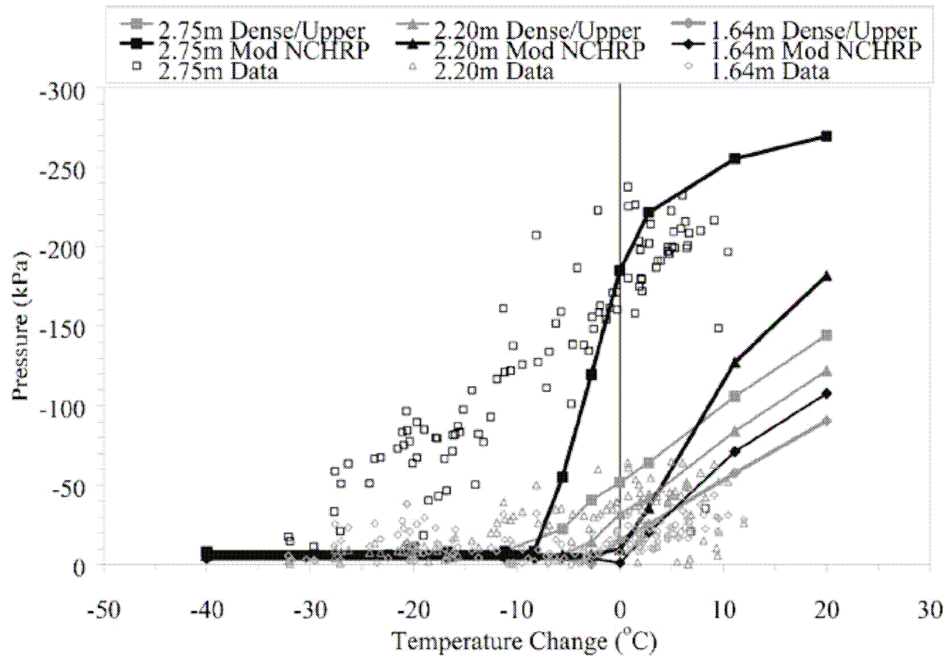

Figure 23. Average earth pressure at south abutment vs temp.change, 2004 [37]
*1m=3.2808 ft

Full-scale testing by Penn Department of Transportation

The Pennsylvania State University began a full-scale test in 2002 to evaluate three integral abutment bridges. The project was sponsored by the Pennsylvania Department of Transportation and the Pennsylvania Transportation Institute.

Three prestressed-concrete integral abutment bridges located on I-99, in central Pennsylvania, were instrumented and monitored. They are referred to as: Bridge 203, Bridge 211 and Bridge 222. They are composite slab-on-girder. Four prestressed concrete I-girders were used in each bridge. The number of spans ranges from 1 to 3. The total lengths range from 18.9 m (62 ft) to 52.4 m (172ft). The abutment heights range from 2.56 m (8.4ft) to 4.48 m (14.7ft).
The bridges were instrumented with:

1) extensometers to measure abutment longitudinal displacements,
2) tilt meters to measure abutment and girder rotations,
3) pressure cells to measure abutment earth pressures from backfill,
4) strain gages to measure bending and axial strain of girders and piles, and
5) sister bar gages to measure axial strain of approach slabs.

Figure 24, Figure 25, and Figure 26 show the lateral soil stiffness for the three bridges, respectively. The data shows that the lateral soil stiffness is different for each of the three bridges, and is inversely proportional to the bridge length. This was explained by the observation that the lateral soil stiffness is essentially a secant stiffness of a nonlinear stress-strain relation, which is generally smaller when deformation gets larger.
Only bridge 203 was instrumented to record earth pressure for three continuous years. This pressure is shown as a function of time in Figure 27 and Figure 28.[38] The maximum pressure behind the abutment for each year keeps increasing for three continuous year.

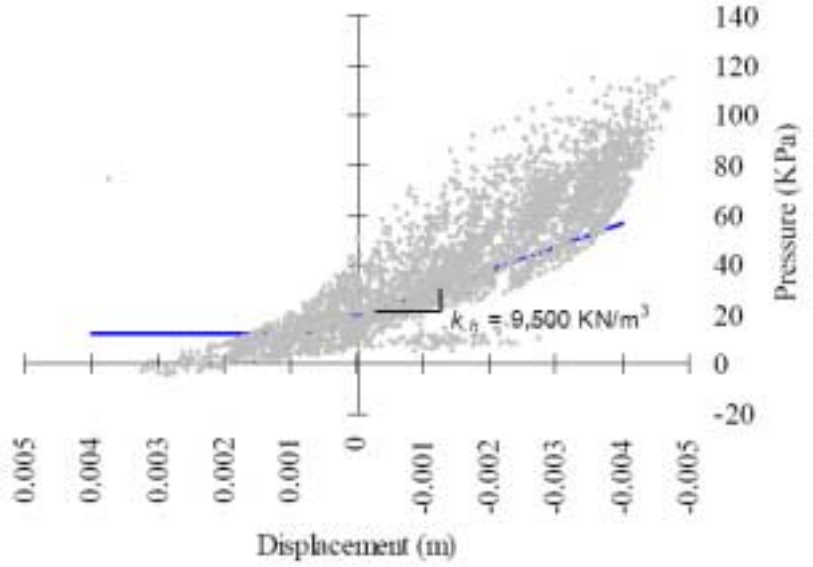

Figure 24. Lateral Soil Stiffness for Bridge 203 [36]

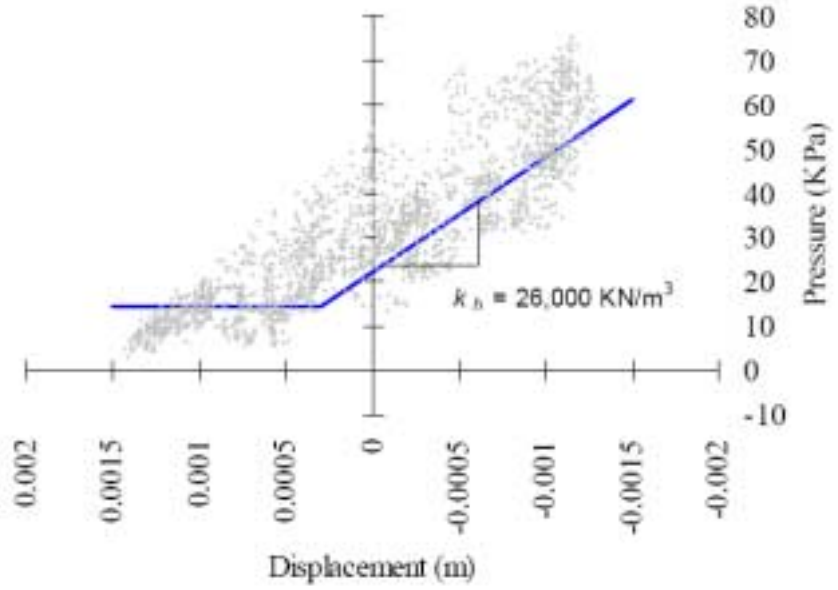

Figure 25. Lateral Soil Stiffness for Bridge 211 [36]

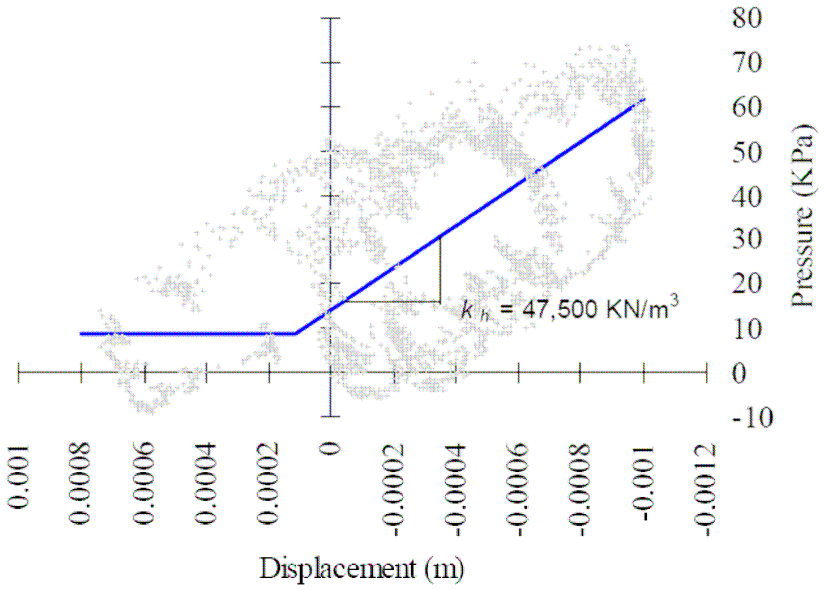

Figure 26. Lateral Soil Stiffness for Bridge 222 [36]

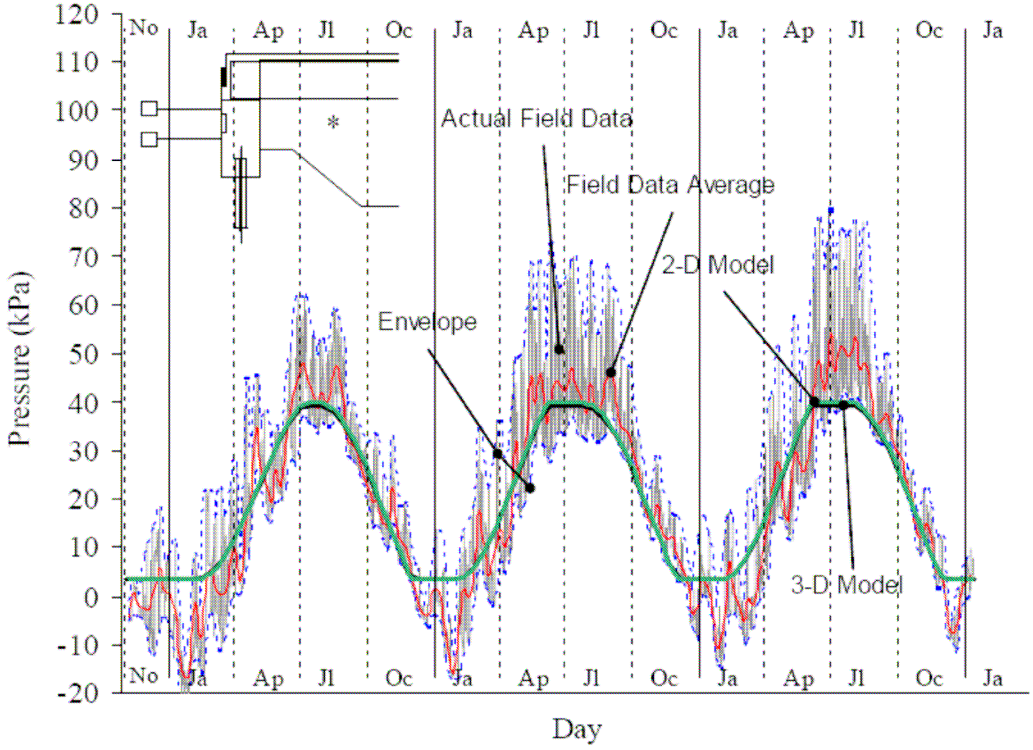

Figure 27. Top Elevation Pressure Cell Data of Bridge 203[36]

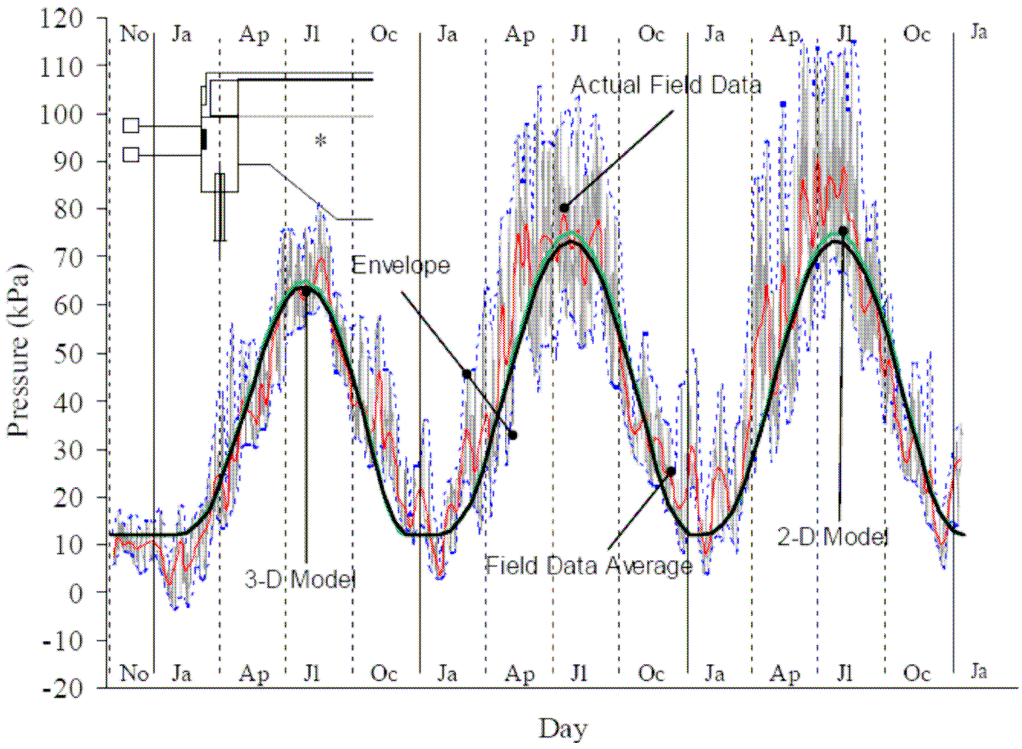

Figure 28. Bottom Elevation Pressure Cell Data of Bridge 203[36]

Summary

All of the full-scale tests performed in Massachusetts and Pennsylvania revealed an earth pressure build-up. None of the tests were conducted long enough to find out when this increase slows down or reaches steady state.

In Massachusetts, the field record pressure behind abutment at different depths is compared with the temperature changes as shown in Figure 22 and Figure 23. In both figures, the maximum pressure didn't occur at the maximum temperature changes. Since the collected data shows that the abutment displacement is proportional to the temperature changes, one can say that the maximum pressure didn't occur at the maximum abutment displacement. The same was observed from the testing at Pennsylvania. Figures 24 to 26 presents the abutment displacement versus pressure. All of them show that the maximum displacement did not correspond to the maximum pressure. The data at Scotch Road shows the same trend, and it will be discussed in the next chapter.

CHAPTER 5- FULL-SCALE TESTING OF SCOTCH-ROAD BRIDGE

Bridge Description

The Scotch Road Integral Abutment Bridge crosses over I-95 in Trenton, New Jersey. It is a 300 ft (90.0m)-long, two-span continuous bridge with a 15^{o} skew angle. The steel superstructure is made of 10 high performance steel girders and is supported on reinforced concrete integral abutments each of which rests on 19 HP 14x102 (360x152) steel piles. The abutments are 3 ft (0.9m) wide and 11 ft (3.35m) deep. The soil behind the abutment is porous compacted fill, whose gradation limits, as specified by AASHTO T 27, are as shown in Table 3:

Table 3- AASHTO gradation specification for I-9 porous fill[32]

Sieve Size*	Percent Passing
150 mm	100
75 mm	70-100
4.75 mm	30-80
425 µm	0-25
75 µm	0-10

* 1m=3.2808ft

Instrumentation

General

The abutment and foundation piles supporting the Scotch Road Bridge were instrumented. Nine soil pressure cells were used to get the horizontal soil pressure behind the abutment, as shown in Figure 29. Two inclinometers were placed on the abutment to measure the rotations at the superstructure/abutment connection. Two gages were specifically constructed to obtain the longitudinal displacements of the superstructure. These gages are placed where the approach slab rests on the sleeper slab. Assuming that the roadway is not moving with temperature, these gages record the absolute displacement of the bridge. Construction details, such as the placement of a frictionless membrane

between the approach slab and the fill, ensures that the approach slab moves rigidly as the superstructure expands due to temperature.[39]

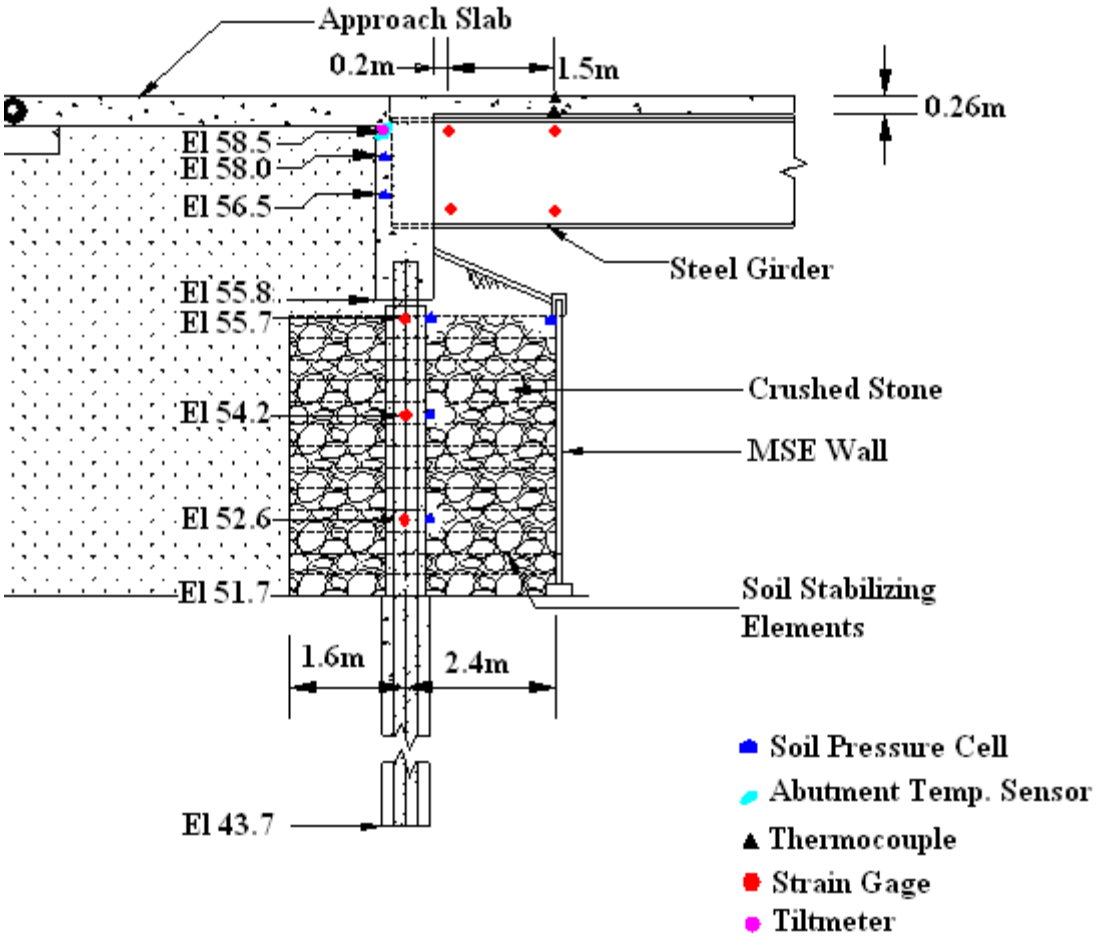

Figure 29. Plan view of instrumentation[39]

Soil Pressure Sensor

The soil pressure cells, shown in Figure 30, were manufactured by Sensing Systems (2002) and calibrated in the laboratory before being installed on site.[40] They constitute as a thin, flat plate, 4-in (10cm) in diameter and 5/8-in (1.6cm) in thickness, which houses several strain gages. A 3-in (7.6cm) diameter pressure-sensing element was utilized to provide the soil pressure area sample. The pressure-sensing element was made of 630 stainless steel, heat-treated to H900 condition. Eight individual strain gages were bonded to the sensing element at the center, at the outside diameter and along four equally spaced radial lines. The eight strain gages were wired into a single Wheat stone bridge circuit. The

bridge circuit output signal was designed to be insensitive to temperature changes and mounting configuration.

Figure 30. Soil pressure gage[41]

Each soil pressure sensor was calibrated to 50 psi (0.3Mpa) by application of hydrostatic pressure on the face of the pressure-sensing element. Steel mounting plates were provided for flush mounting of the soil pressure sensors. A 4-in (10cm) diameter counter bore and a slot were machined into the ground face of the mounting plate to receive the soil pressure sensor and integral cable. The exact location of each soil pressure sensor was measured and marked using optical survey techniques. Loose sand was placed around the sensor within a 0.30 m (1 ft) radius to prevent high stress concentrations due to the coarse backfill.

Locations of the soil pressure cells

The pressure cells were installed behind each of Piles 3 and 9 at identical elevations of 56.5, and 58.0 m during Stage I construction, while Pile 14 was instrumented at elevations of 57.17, 57.84 and 58.5m, during Stage II construction. The gages are shown in Figure 31. It should be noted that Piles 3 and 9 are on the side of the bridge skew that makes an acute angle with the

centerline, while Pile 14 is located on the side that is at an obtuse angle with the centerline. As a result, Piles 9 and 3 experience greater pressures.

A data acquisition system was installed and connected to the Stage I sensors in December 2002 and to the Stage II sensors in December 2003. The data acquisition system has continuously recorded soil pressure data at two-hour intervals since initiation of the monitoring process in April of 2003. The data was downloaded once a month to office computers. All soil pressure sensors have successfully recorded high quality data throughout the monitoring period.

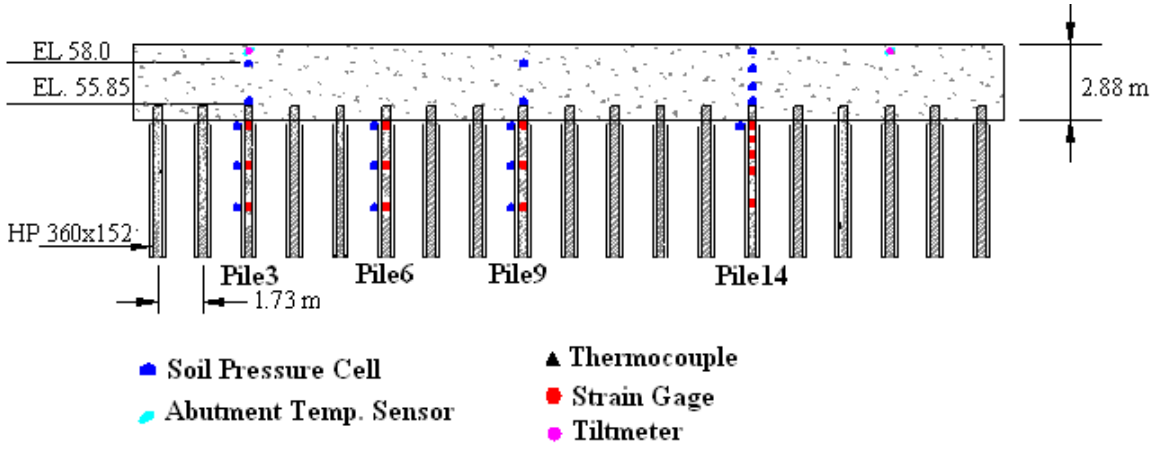

Figure 31. Side-view of instrumentation [39]

Recorded data on the Scotch Road Integral Abutment

Recorded displacement of the integral abutment

The displacement of the integral abutment due to the thermal variation is predicted from Equation 11 as $\Delta=1/2L\alpha\Delta T$, where L is the length of the continuous bridge; α is the coefficient of thermal expansion; ΔT *is* the difference between the temperature during construction and the maximum (or minimum) temperature expected at the site. Figure 32 shows the recorded displacement in the Scotch Road bridge is proportional to the temperature variations, as expected.

Integral abutments are affected by both maximum and minimum daily, and seasonal temperature variations. The temperature increases gradually during the day, which results in the expansion of the bridge superstructure, and hence,

the passive movement of the abutment. The cycle is reversed at night, when the temperature decreases and the active movement of the abutment takes place. Figure 33 shows the displacement of the superstructure over 24 hours period.

The daily cycles are repeated constantly. However over the year, we do not observe an exact correlation of displacement and pressure due to the fact that the soil is not an elastic medium. Figure 34 shows the longitudinal displacement at the top of the abutment (measured where the approach slab meets the sleeper slab), Figure 35 shows the rotation of the top of the abutment (measured on the abutment at the stringer base).

The data span a period from April 2003 to June 2006. In general, the displacement increases with temperature from January, reaching its highest value in July, and starts decreasing to its lowest value in January. The same is true for the rotations which correlate well to the displacement readings. However, the rotations are relatively small and do not contribute significantly to the overall movement.

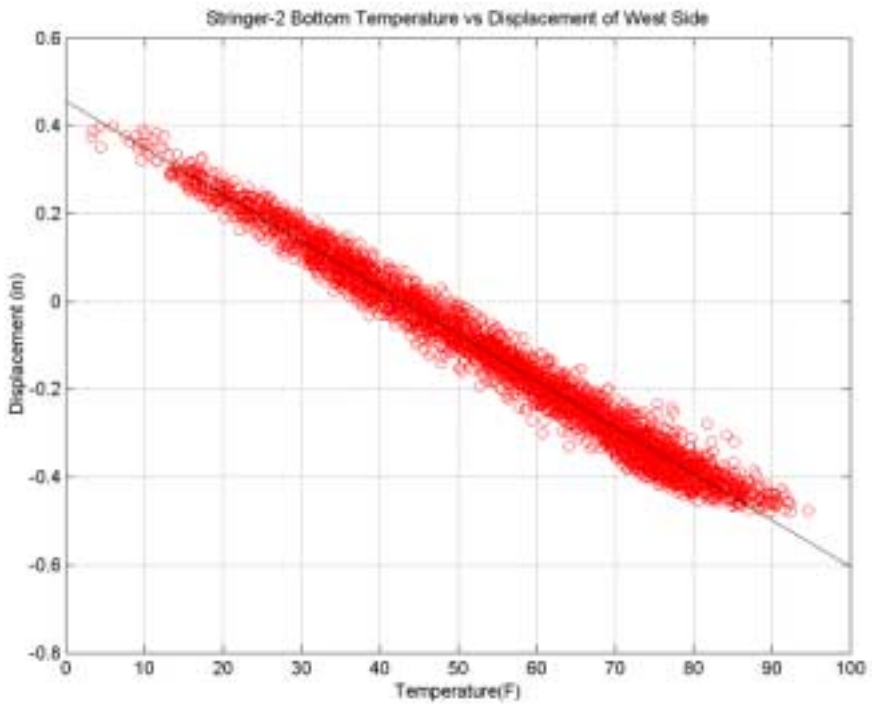

Figure 32. Longitudinal displacement versus temperature. 2003-2006

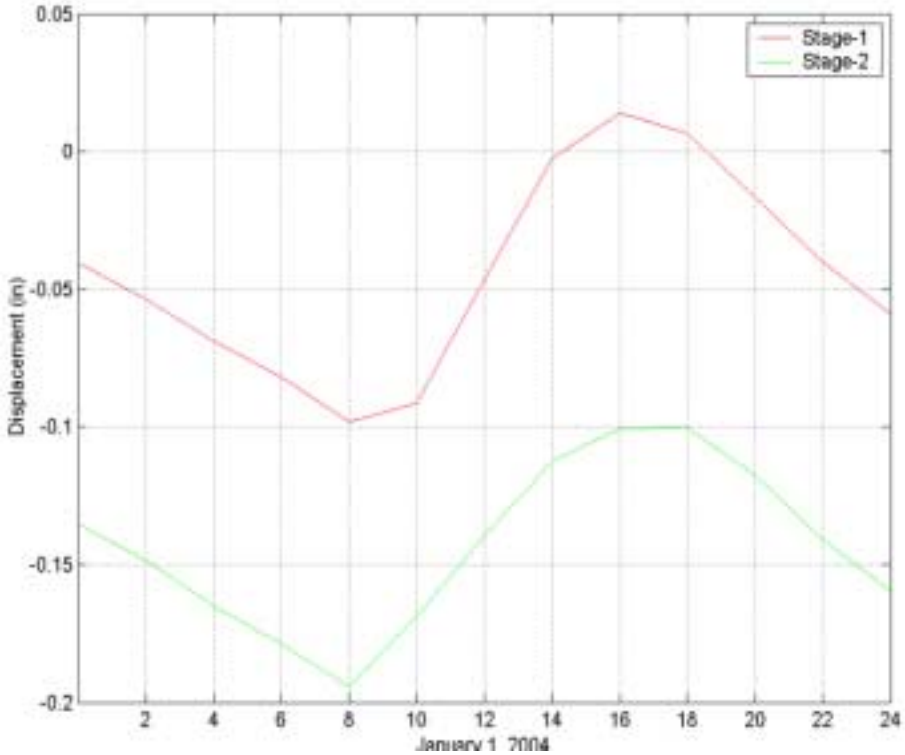

Figure 33. Longitudinal displacement of bridge over 24 hours, January 1, 2004[42]

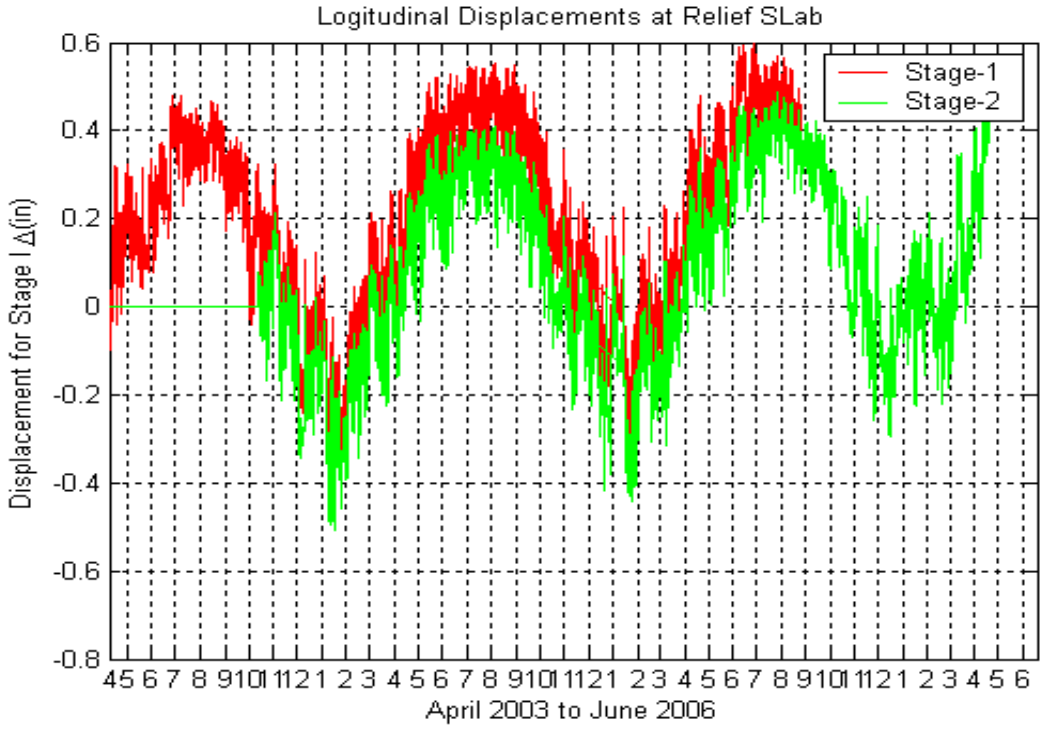

Figure 34. Longitudinal displacement at the sleeper slab.

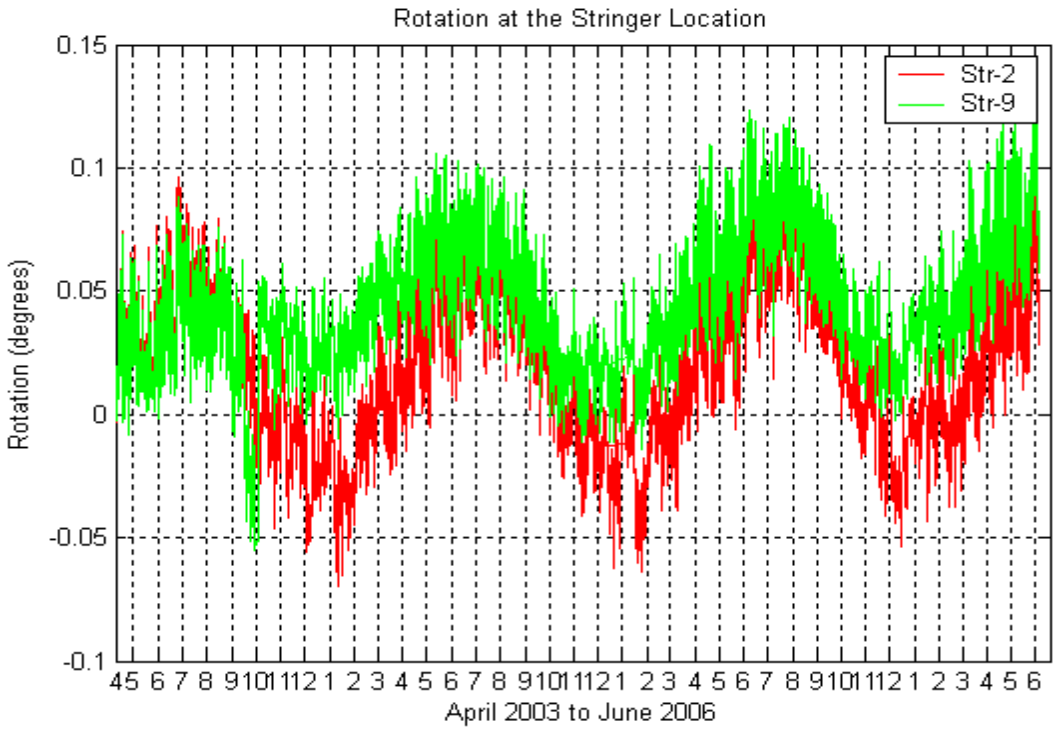

Figure 35. Rotation of the abutment at the stinger connection.

Recorded soil pressure behind the Integral Abutment

General

Sensors on Pile 3 and Pile 9 were placed at Elevations 56.5m and 58.0m respectively, and recorded data from April 2003 to June 2006 (Stage I). Sensors on Pile 14 were placed at Elevations 57.17m, 57.84m and 58.5m respectively, and recorded data from October 2003 to July 2006 (Stage II).

Figure 36 shows the pressure development behind the abutment due to the thermally induced displacement over a period of 24 hours. Starting at time 00:00 up to 8:00 the displacement decreases due to the night temperatures, pulling the abutment away from the soil. This is reflected in the presence of active pressure behind the abutment. From 8:00 to 16:00 the day temperature increases, pushing the abutment against the soil and creating the highest passive pressure at the maximum displacement at 16:00. From 16:00 to 24:00 the abutment starts pulling away relieving the pressure, which seems to dissipate and reach active values

around midnight. Figure 37 and Figure 38 show this correlation over a one-month period.

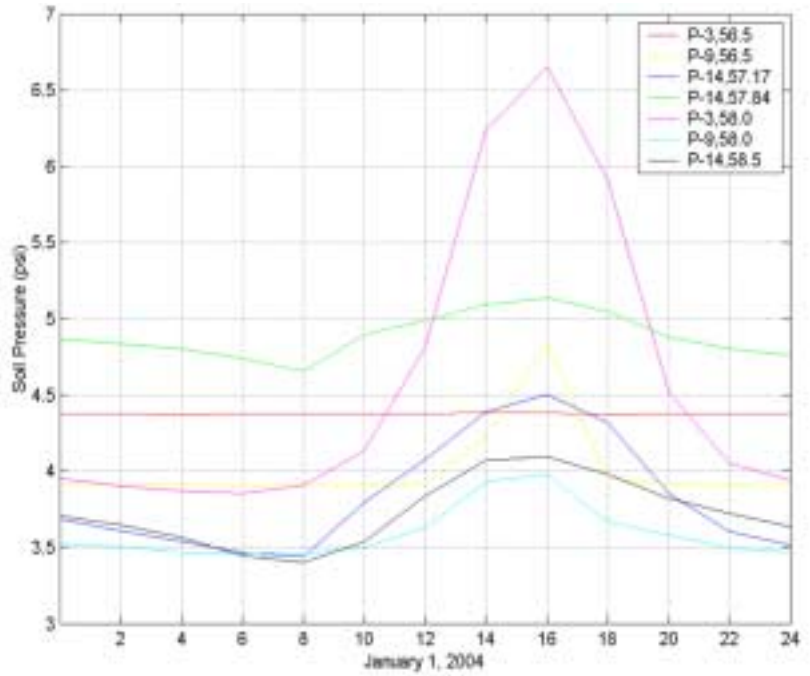

Figure 36. Soil pressure behind abutment over 24 hours, January 1, 2004[42]

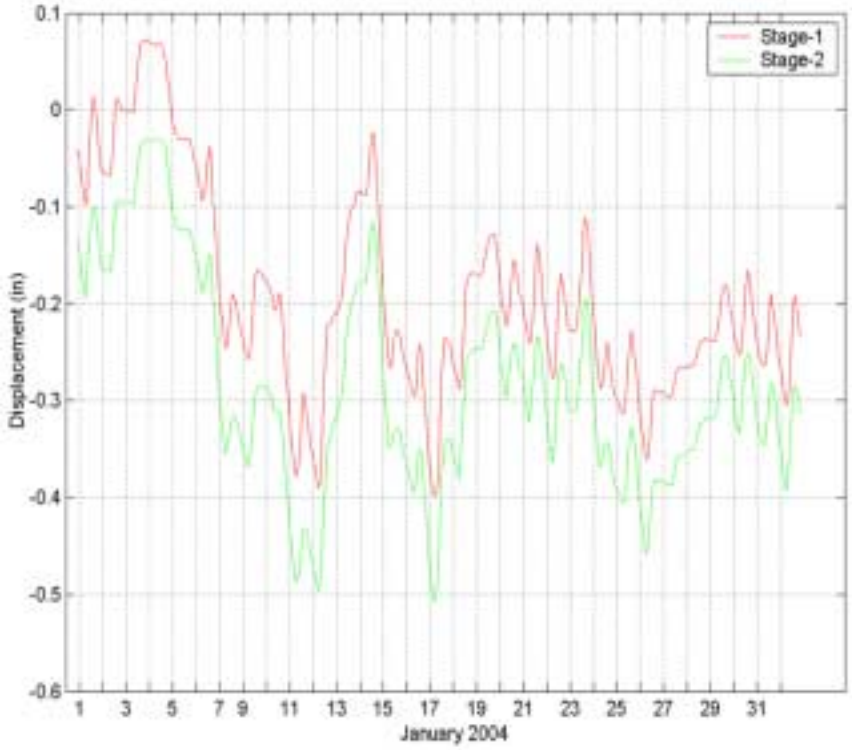

Figure 37. Longitudinal displacement of bridge over one month, January 2004[42]

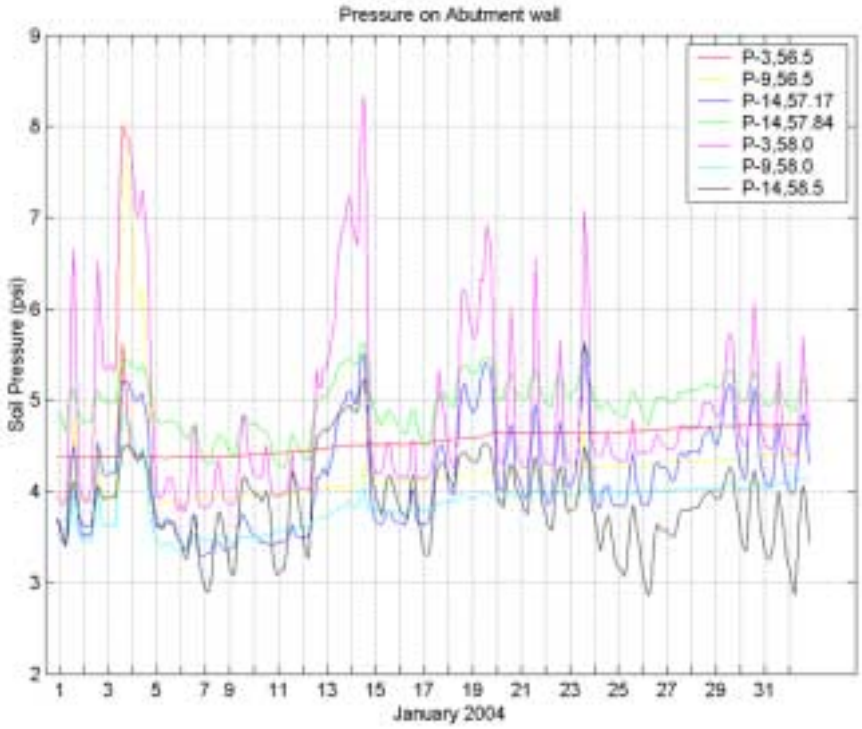

Figure 38. Soil Pressure behind abutment over one month, January 2004[42]

Recorded soil pressure at Pile 3 and Pile 9

Figure 39 to Figure 43 show the recorded earth pressure at each sensor for the duration of the project. The field data reveals that the lateral pressure keeps increasing for the first three years reaching a steady state at the fourth year.

In contrast to the displacement, the pressure seems to be the greatest at the very beginnings of temperature increases in February, reaches its highest value of the year around April and decreases to an average value by July. As the displacement reverses direction in July, the pressure starts to decrease. We can deduce from this that the soil is in its densest state at the end of the seasonal active cycle and it behaves as dense sand in shear as the temperatures start to climb and the abutment starts pushing on the soil.

The built up of pressure from year to year is a result of the changes in soil density and soil fabric due to the daily cyclic motion. According to earlier research, the fabric of granular soil changes during the unloading stage, which results in the accretion of permanent plastic deformation, known as strain ratcheting. [19]

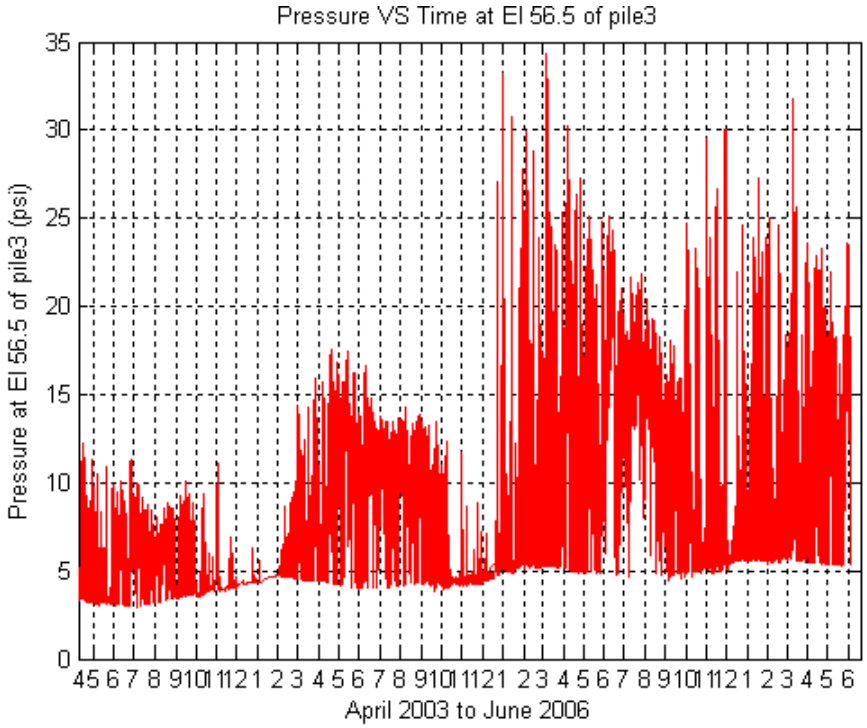

Figure 39. Pressure on the abutment wall at plane of Pile 9, El 56.5 meters

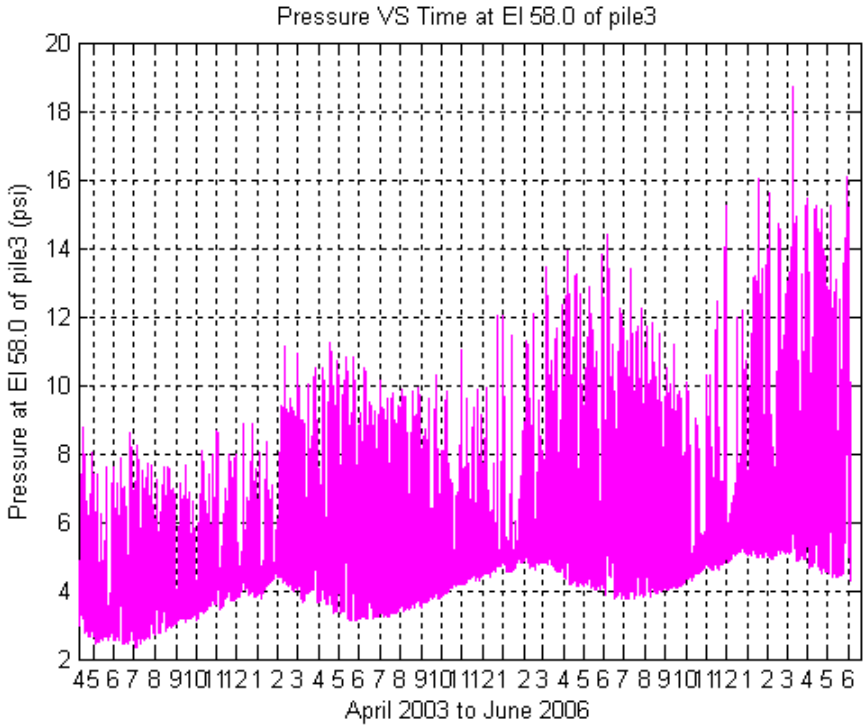

Figure 40. Pressure on the abutment wall at plane of Pile 3, El 58.0 meters

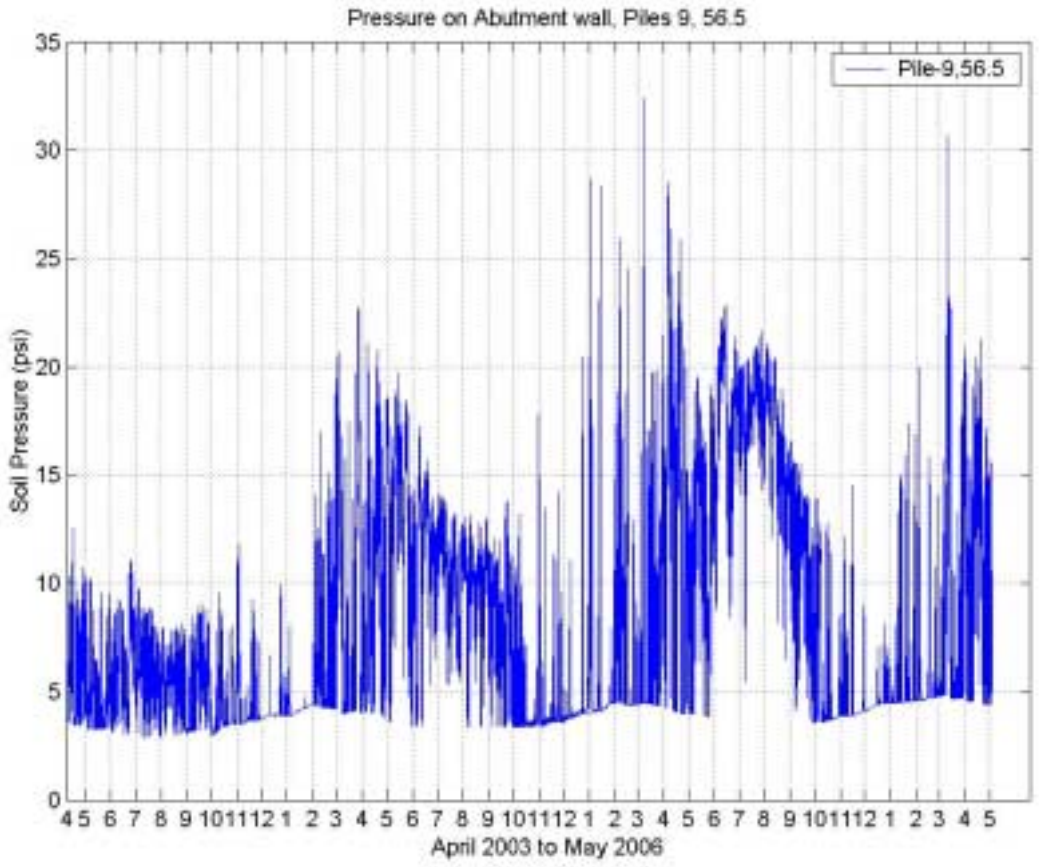

Figure 41. Pressure on the abutment wall at plane of Pile 9, EL 56.5 meters

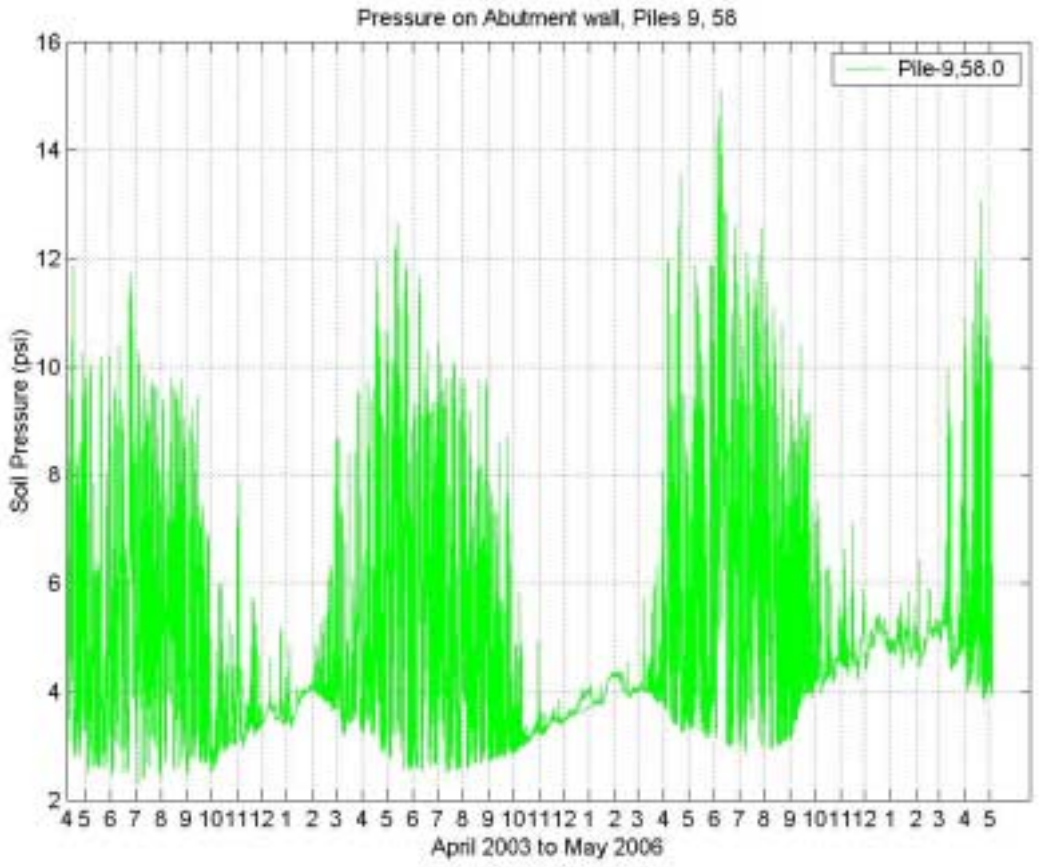

Figure 42. Pressure on the abutment wall at plane of Pile 9, EL 58 meters

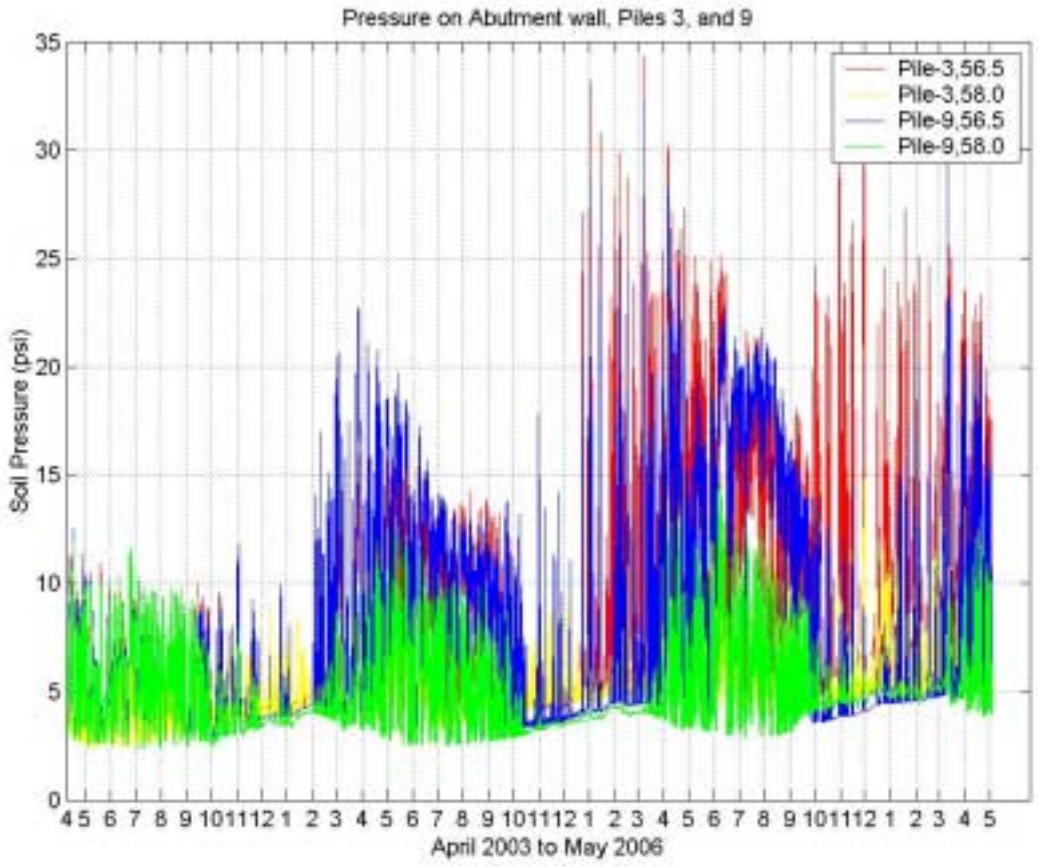

Figure 43 Pressure on the abutment wall at section of Piles 3 and 9

Effects of Skew

Piles 3 and 9 are on the side of the bridge that makes an acute angle with the centerline. As such, they experience greater pressures during passive movements that measured at Pile 14, which is located on the obtuse angle of the skew. Figure 44, Figure 45 and Figure 46 shows the recorded earth pressure at each sensor from October 2003 to June 2006, measured at Pile 14. The increase of pressure with each year is evident. However the pressure is much smaller, and for that reason, this data was not included in the study of the K_h factor.

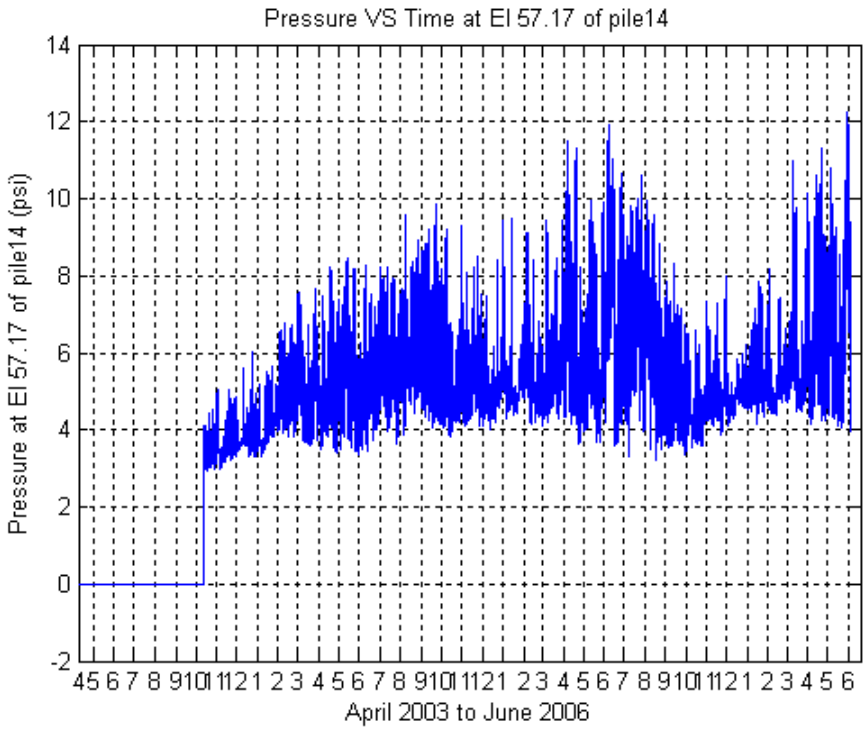

Figure 44. Soil pressure at El 57.17 of pile 14. Stage II construction.

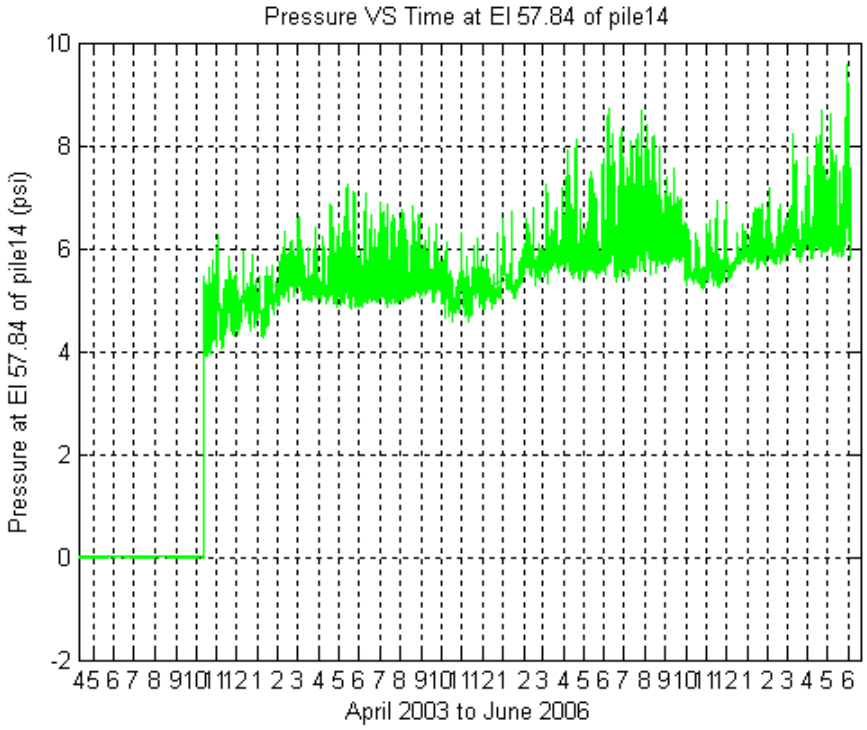

Figure 45. Soil pressure at El 57.84 of pile 14. Stage II construction.

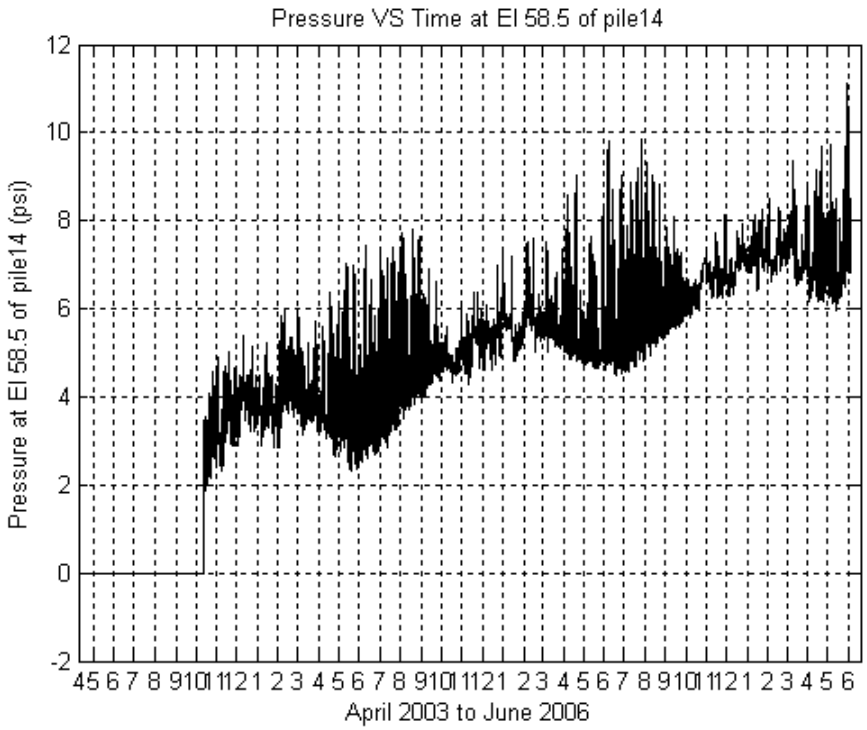

Figure 46. Soil pressure at El 58.5 of pile 14. Stage II construction

CHAPTER 6- DATA ANALYSIS AND COMPARISON WITH LITERATURE

In this section, data from the Scotch Road Bridge is plotted along the work of other researchers to evaluate the effect of abutment movement in the development of a horizontal pressure coefficient K_h. To compare the data recorded in the Scotch Road Bridge with the literature, the pressure coefficient is calculated using a constant soil density of 125pcf. Any changes in density during the cyclic disturbance of the soil are reflected in the change of pressure, thus the change of K_h. In addition, a new at-rest position is assigned to the abutment every winter. Passive displacements are calculated every year as the displacement of the bridge from its winter position.

The horizontal pressure coefficient extracted from the data is compared with the literature in Figure 48 to Figure 63. These figures contain information from the Massachusetts Bridge Manual, [33] the laboratory work performed in England [19], and the earth pressure coefficient curves for dense sand developed by NCHRP [43] and reproduced in Figure 47.

The data shows that in the first two years, the pressures are low, more in line of what one would expect for loose sands. By the fourth year, the coefficient is closer to that predicted by the NCHRP for dense sands.

For small displacements, the coefficient increases with displacement and can be predicted by the NCHRP proposed K_h value for dense sand. In an integral abutment bridge, this condition is met during the winter months when passive displacements are small and the soil is at its densest state. At larger displacements, the K_h factor in the integral abutment bridge does not increase with the increasing displacement. Rather, it seems to undergo a small decrease. This condition is met during the summer months when shear resistance has been overcome and the retained soil acts more like looser sand. As a result, during the maximum passive displacements, the K_h factor is smaller than recommended by the NCHRP work.

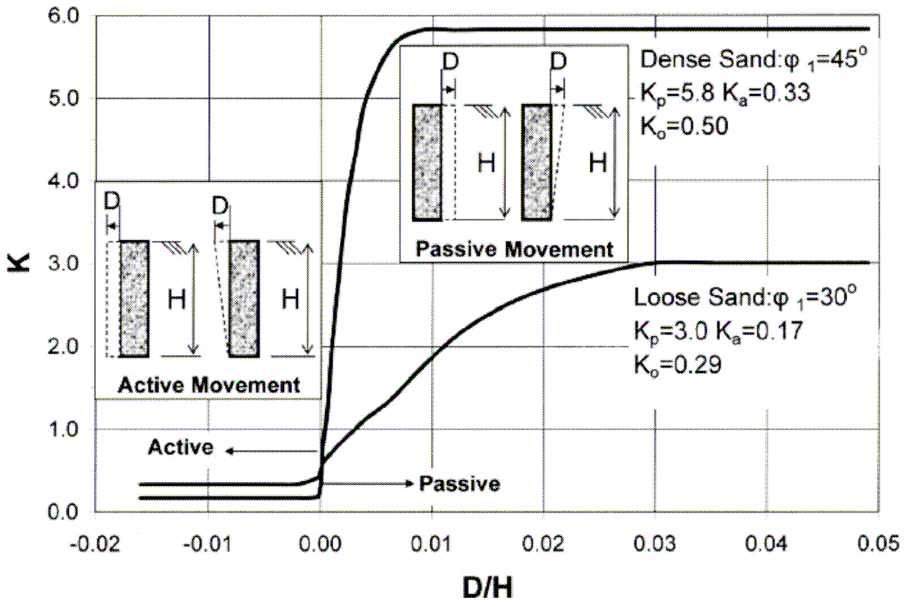

Figure 47. Earth pressure coefficient versus relative wall displacement[43]

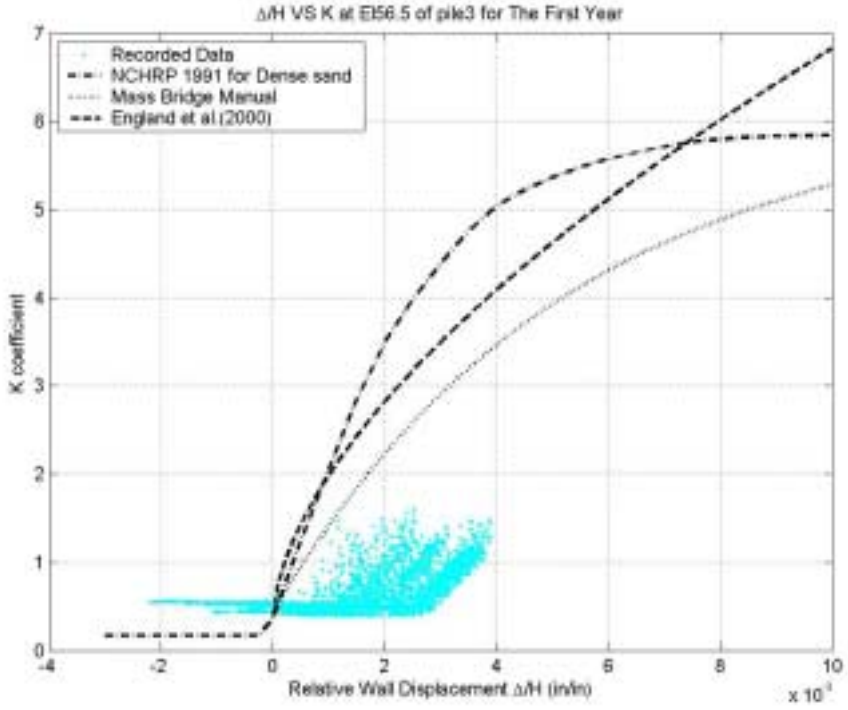

Figure 48. K_h vs Δ/H at El 56.5 of pile 3 for the first year.

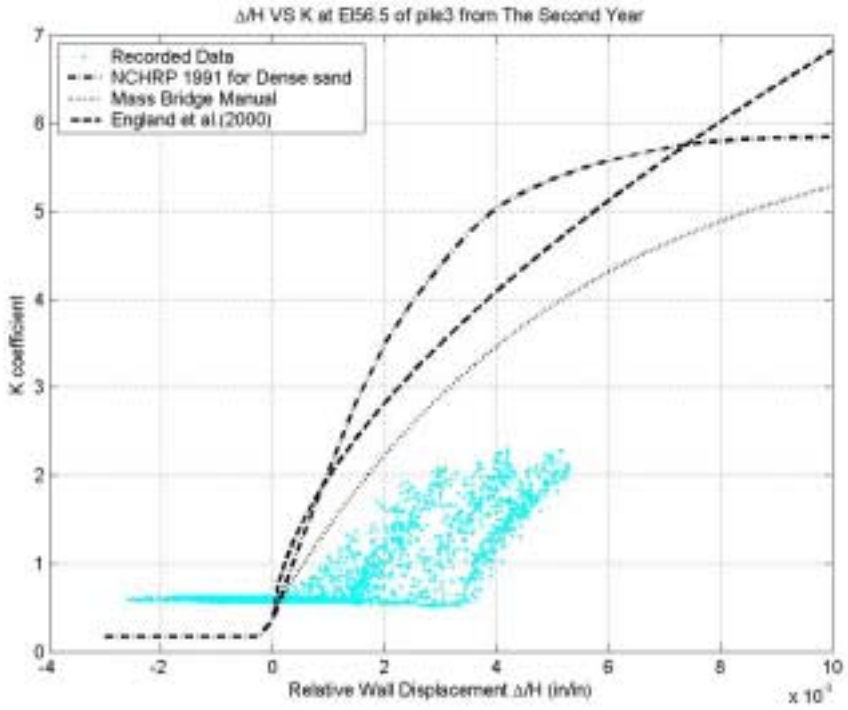

Figure 49. K_h vs Δ/H at El 56.5 of pile 3 for the second year.

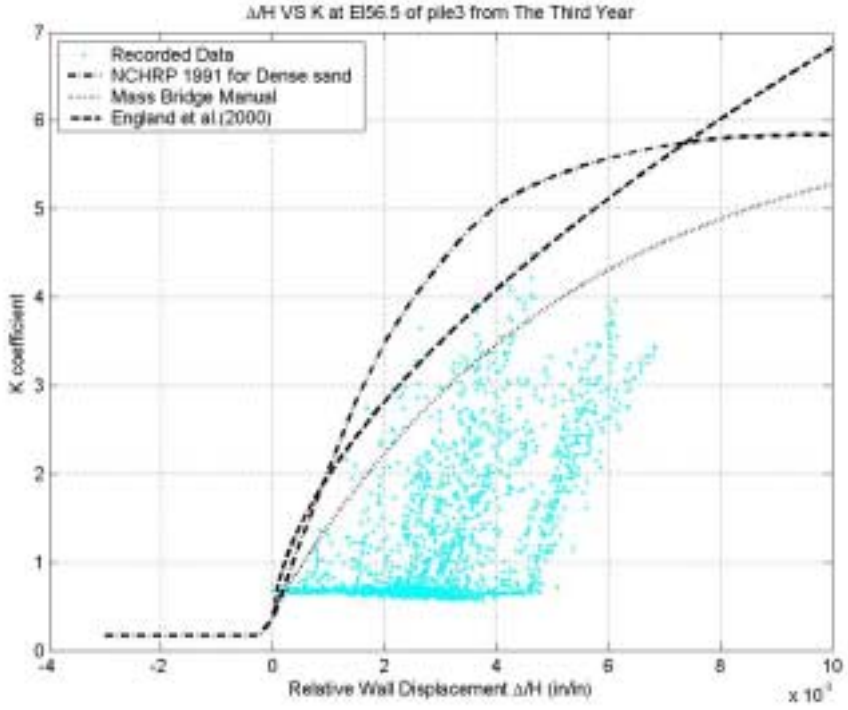

Figure 50. K_h vs Δ/H at El 56.5 of pile 3 for the third year.

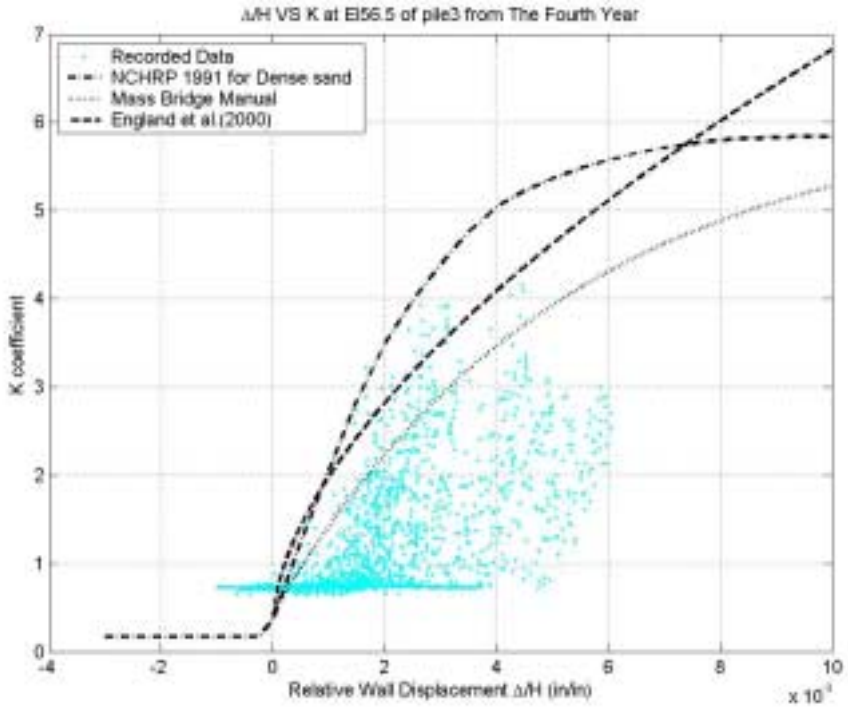

Figure 51. K_h vs Δ/H at El 56.5 of pile 3 for the fourth year.

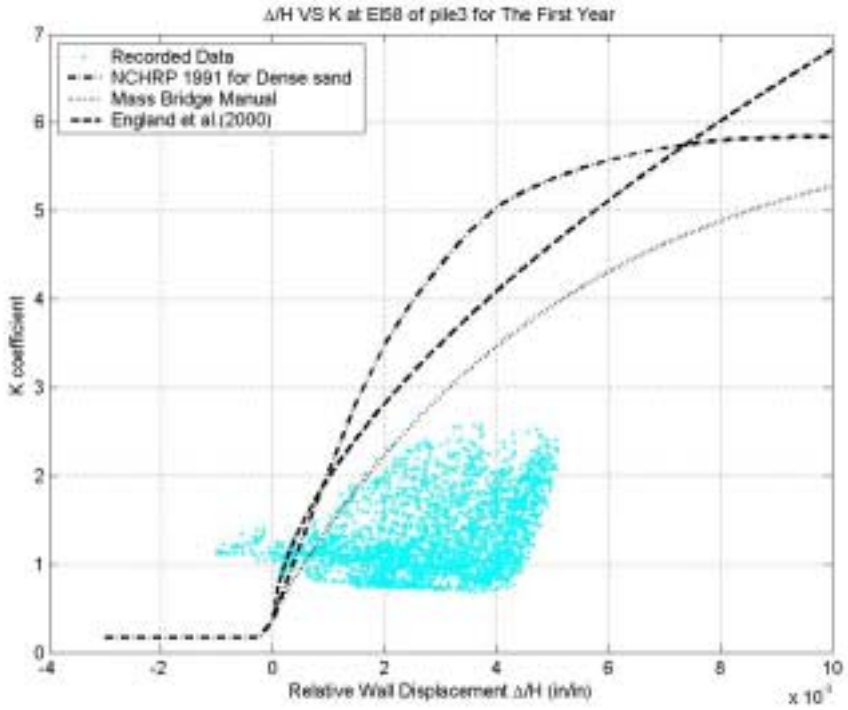

Figure 52. K_h vs Δ/H at El 58.0 of pile 3 for the first year.

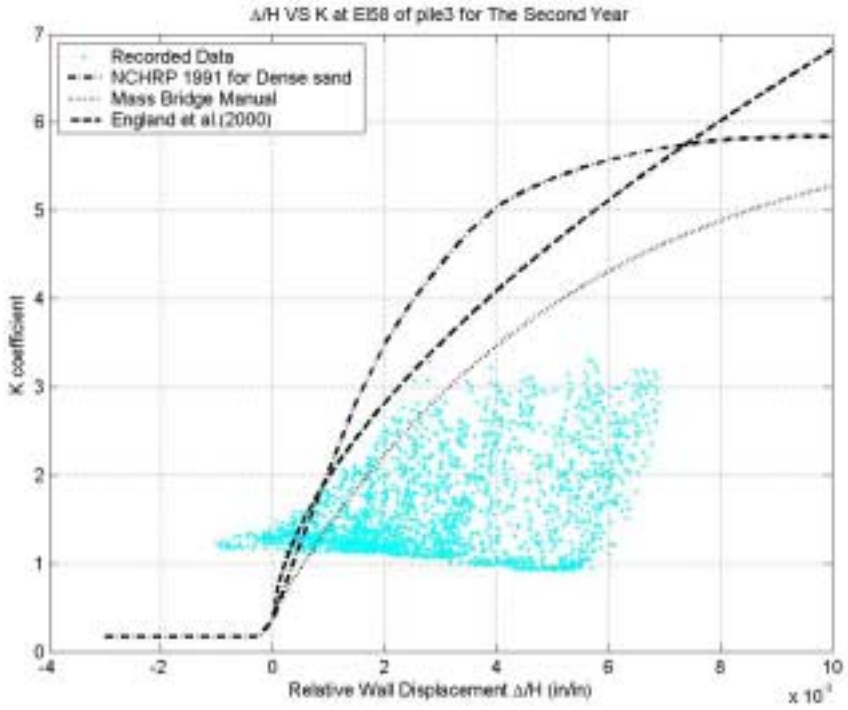

Figure 53. K_h vs Δ/H at El 58.0 of pile 3 for the second year.

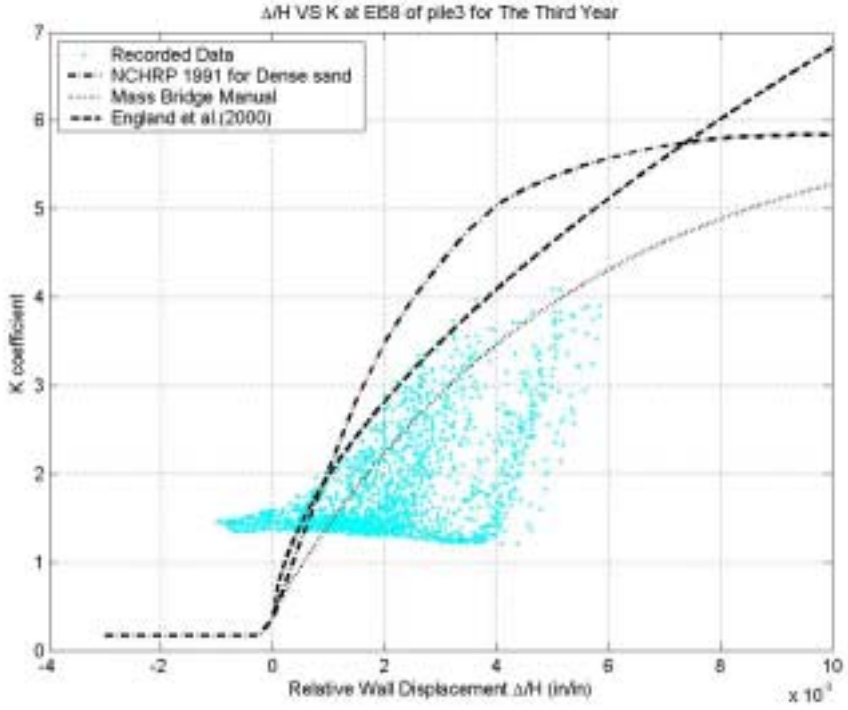

Figure 54. K_h vs Δ/H at El 58.0 of pile 3 for the third year.

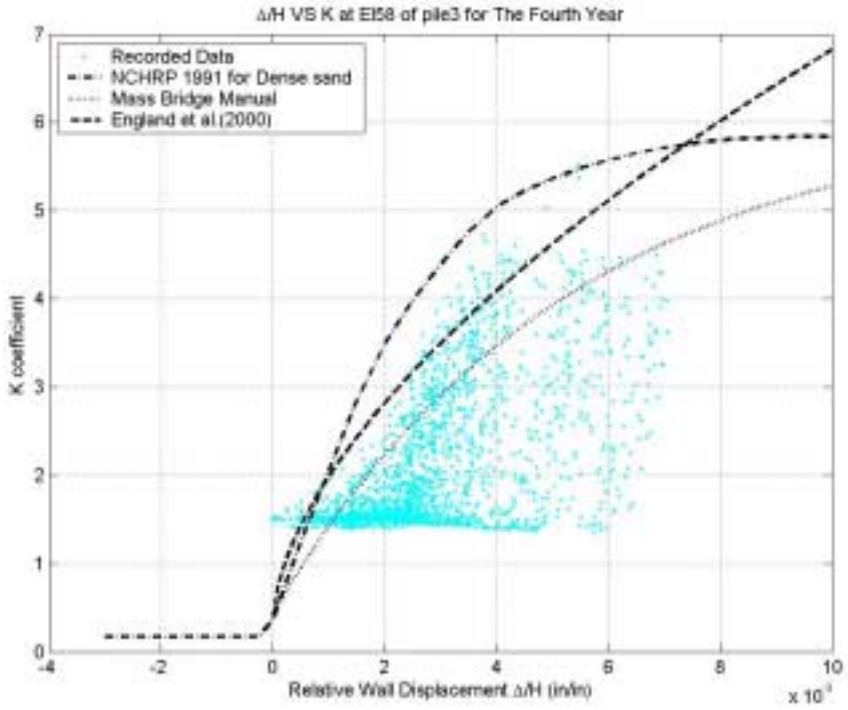

Figure 55. K_h vs Δ/H at El 58.0 of pile 3 for the fourth year.

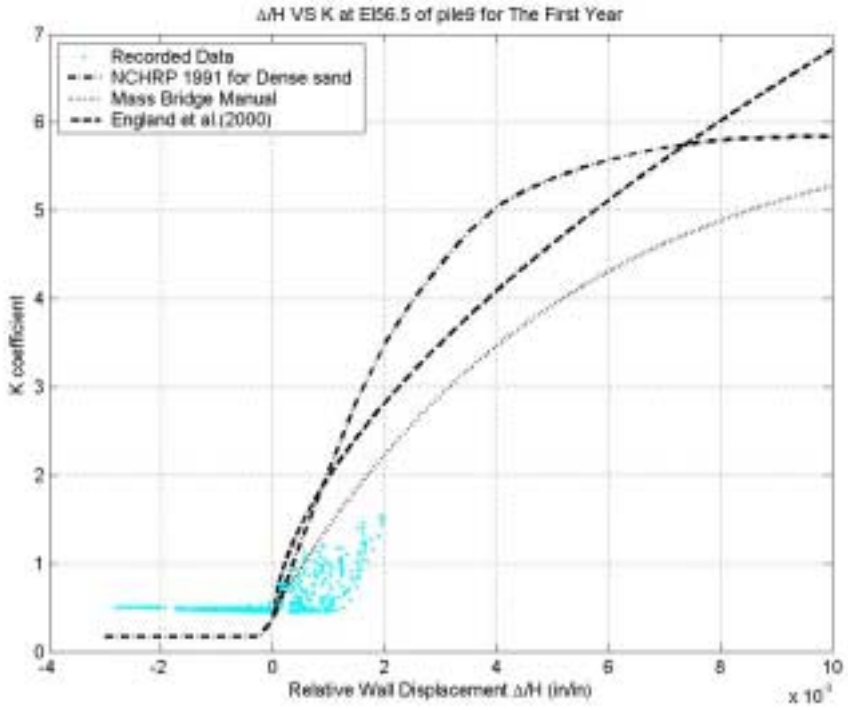

Figure 56. K_h vs Δ/H at El 56.5 of pile 9 for the first year.

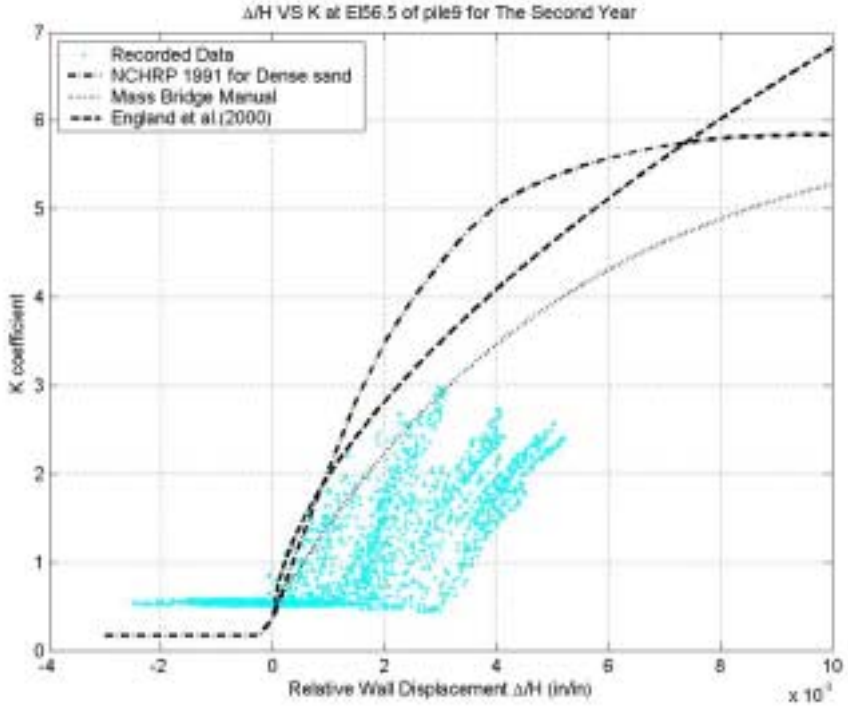

Figure 57. K_h vs Δ/H at El 56.5 of pile 9 for the second year.

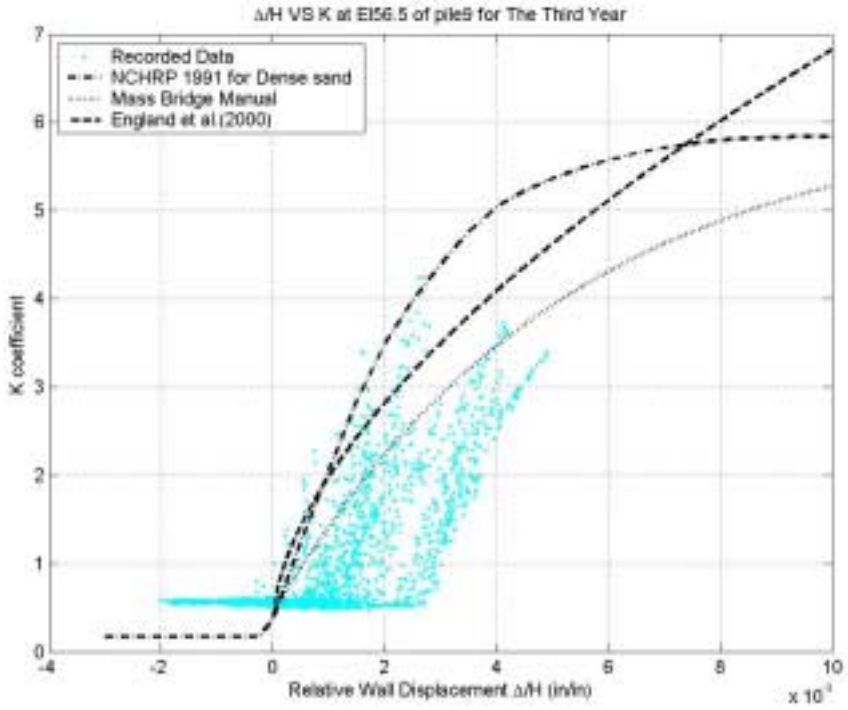

Figure 58. K_h vs Δ/H at El 56.5 of pile 9 for the third year.

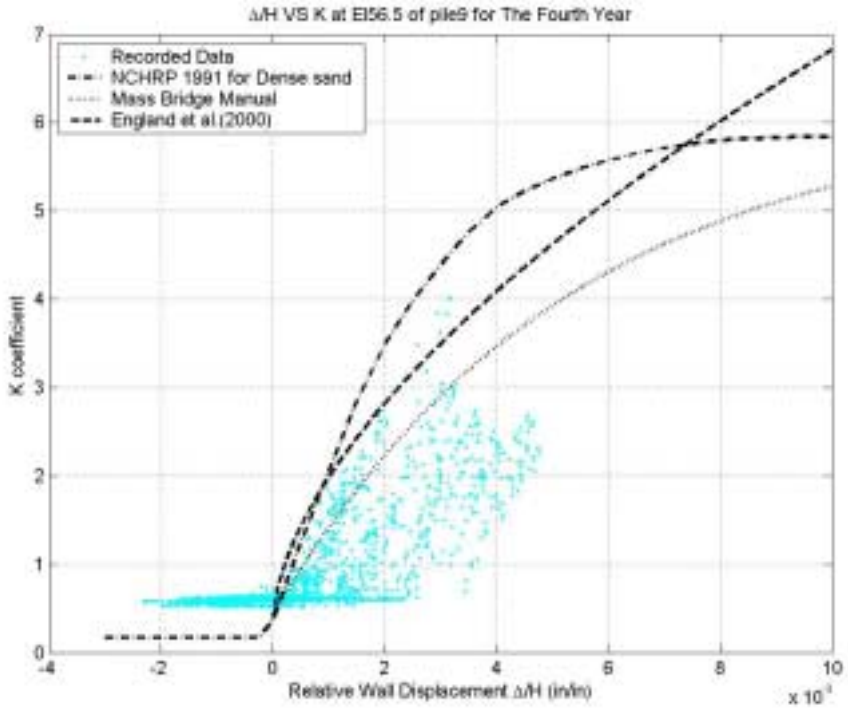

Figure 59. K_h vs Δ/H at El 56.5 of pile 9 for the fourth year.

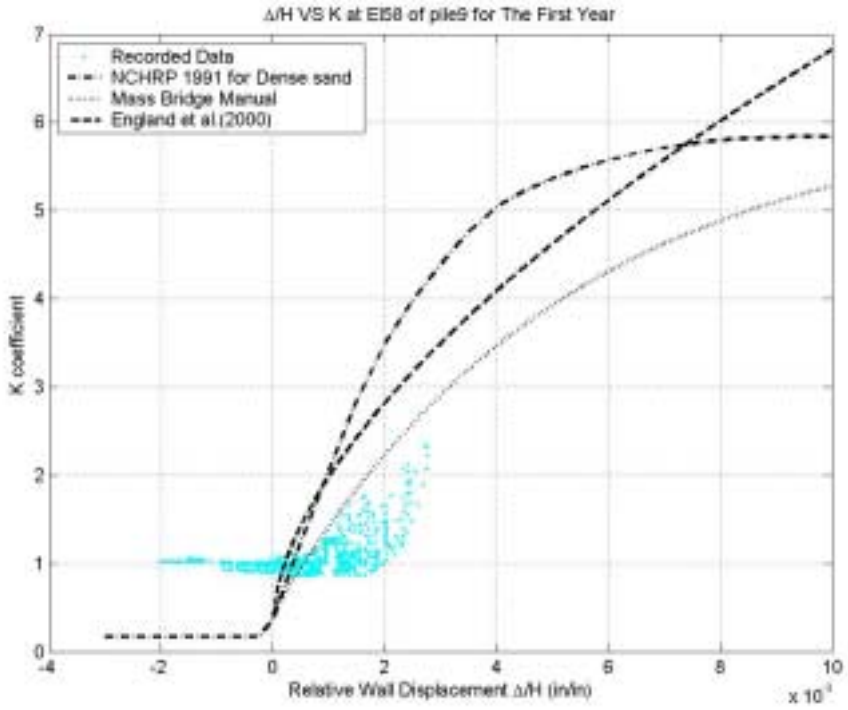

Figure 60. K_h vs Δ/H at El 58.0 of pile 9 for the first year.

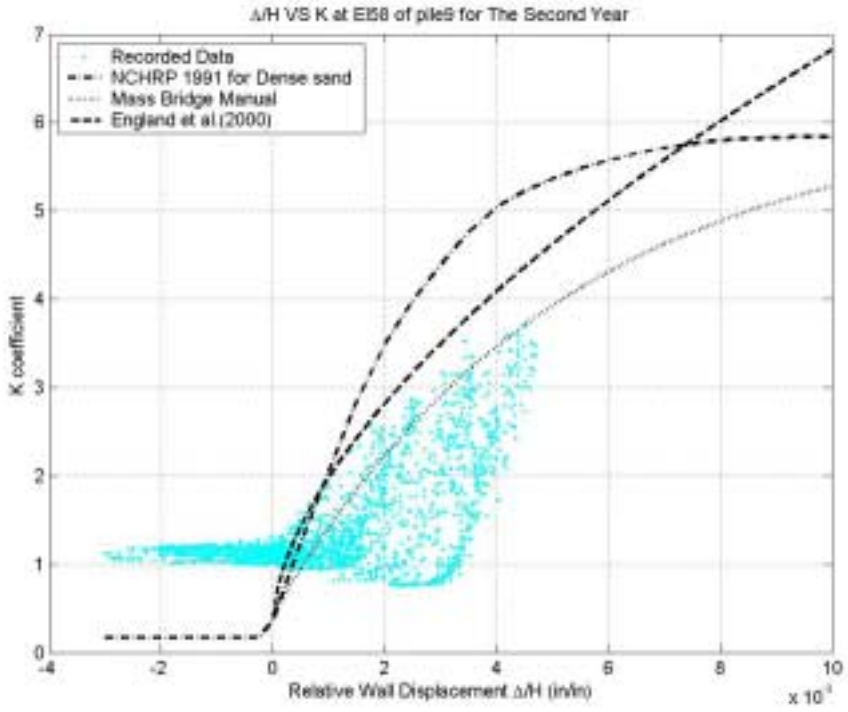

Figure 61. K_h vs Δ/H at El 58.0 of pile 9 for the second year

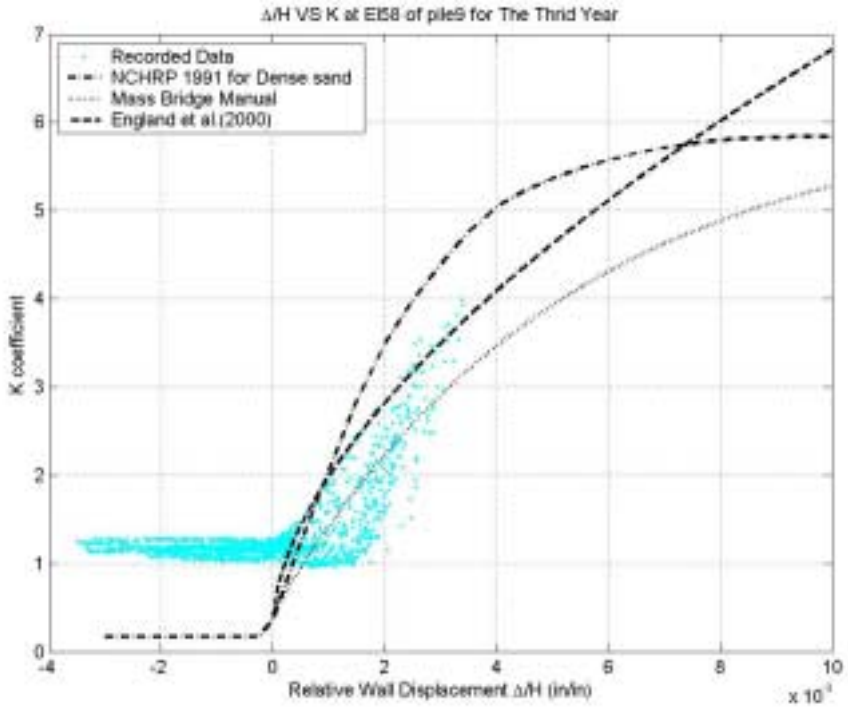

Figure 62. K_h vs Δ/H at El 58.0 of pile 9 for the third year.

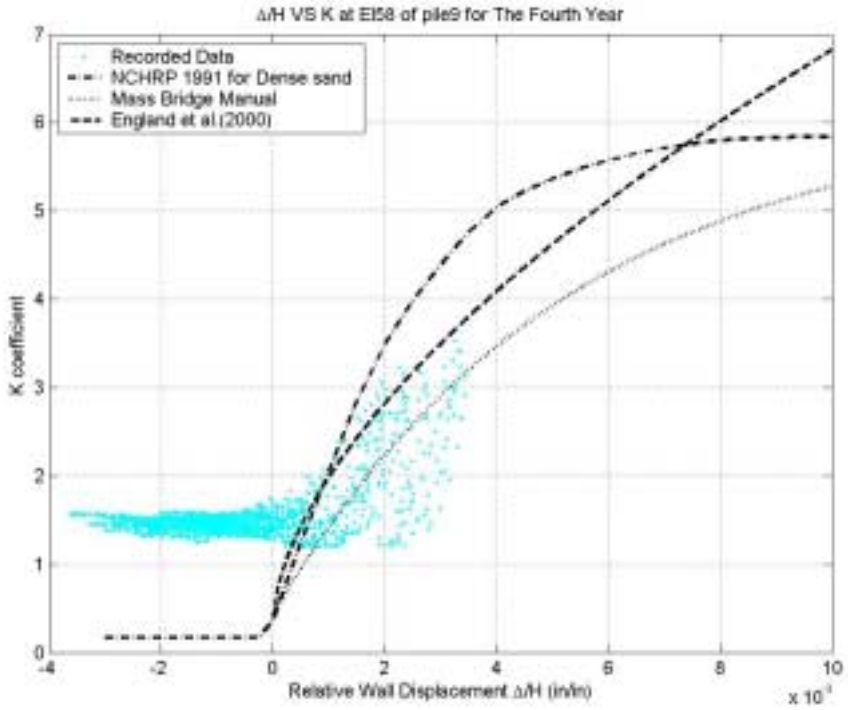

Figure 63. K_h vs Δ/H at El 58.0 of pile 9 for the fourth year

Stress-strain relationship of dense and loose sand

Figure 64 shows the stress-strain relationship for dense and loose sand in shear. At relatively small strains, the dense sand experiences a higher stress than the loose sand. At high strains, both the dense and the loose sands experience the same magnitude of stress.

The soil behind the abutment is observed to behave as dense sand. Figure 65 to Figure 68 show the pressure behind abutment plotted against relative abutment displacement Δ/H for piles 3 and 9. The maximum lateral pressure doesn't occur at the maximum abutment displacement. On the contrary, it occurs at a relatively smaller displacement achieved right after the wintertime. During this time, the abutment is moving toward the soil backfill, and the soil mass is in the densest state. After that, the earth pressure will not increase with the abutment displacement. Rather, it starts to decrease.

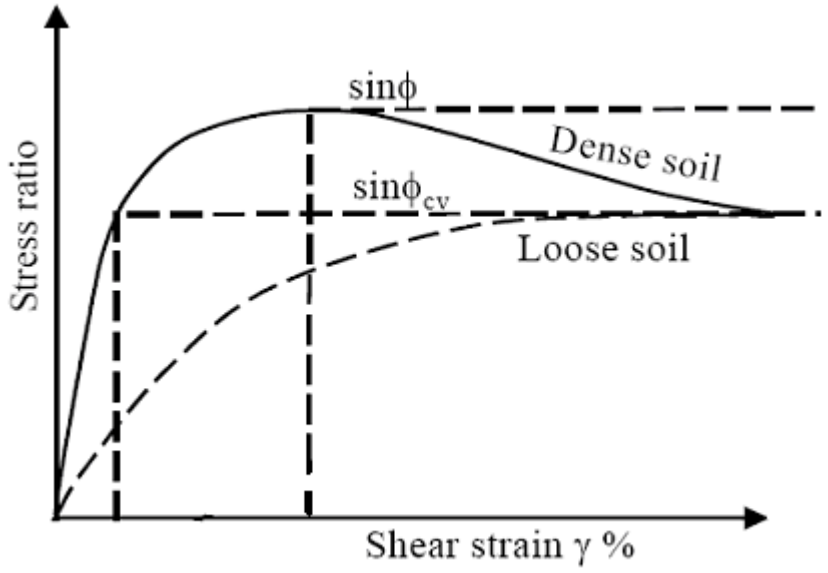

Figure 64. Stress-strain relationship for dense and loose soil [44]

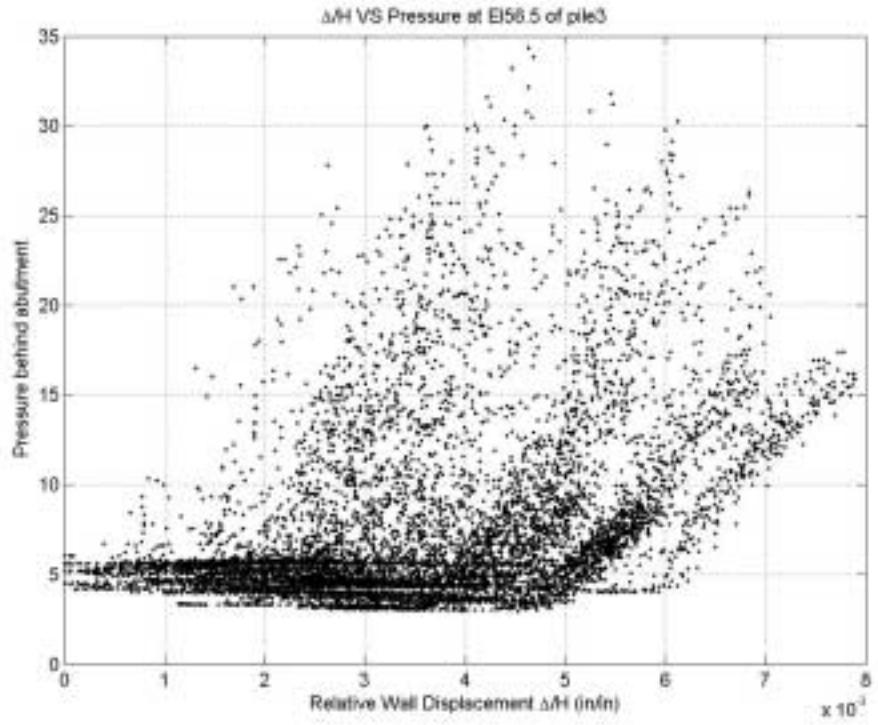

Figure 65. Pressure versus Δ/H at El 56.5 of Pile 3. 2002-2006

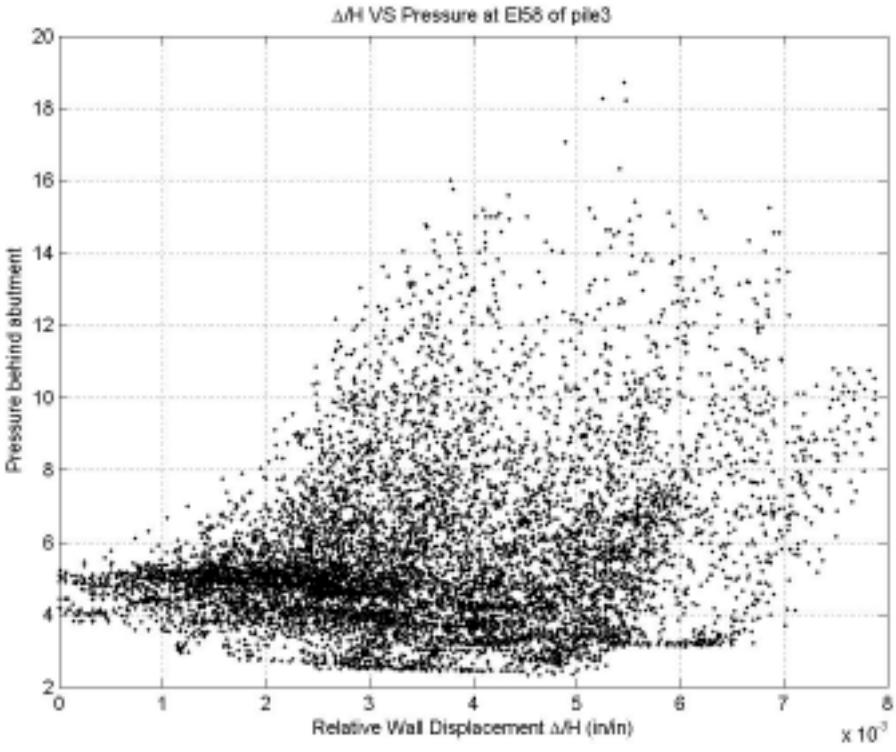

Figure 66. Pressure versus Δ/H at El 58 of Pile 3. 2002-2006

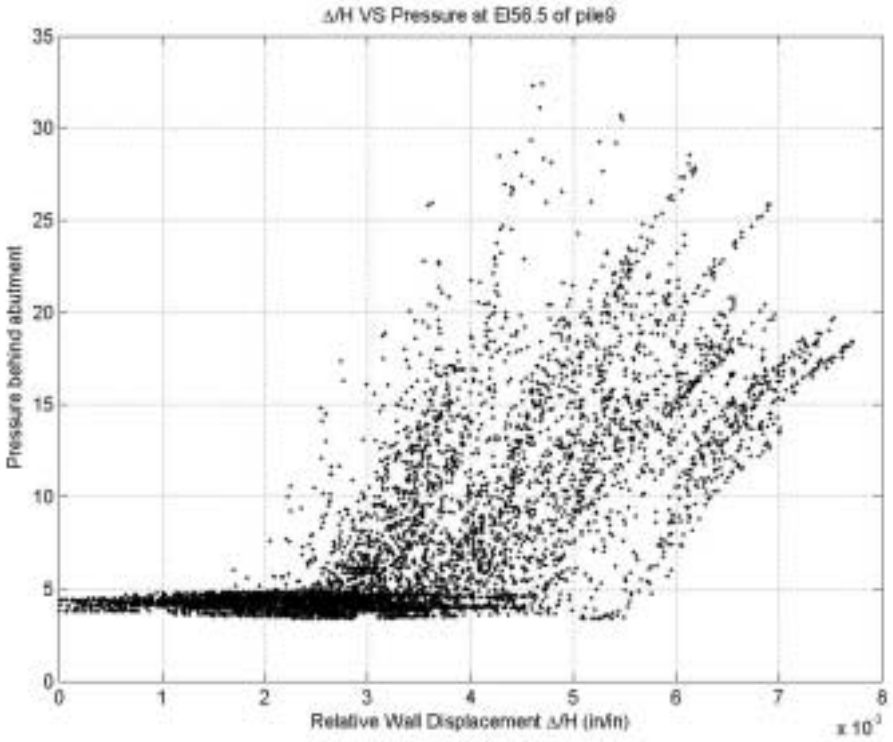

Figure 67. Pressure versus Δ/H at El 56.5 of Pile 9. 2002-2006

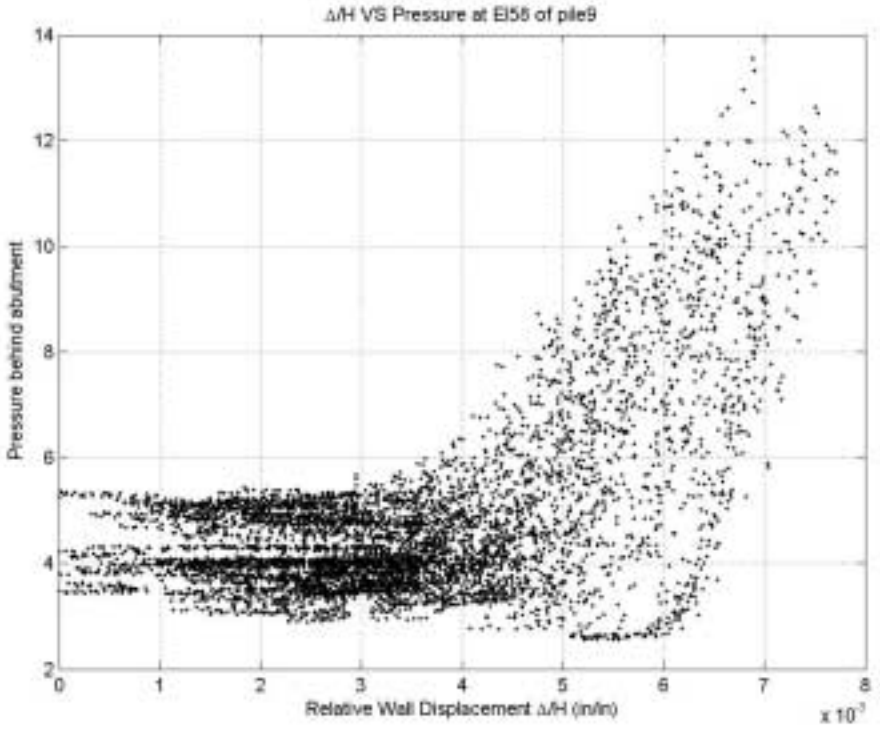

Figure 68. Pressure versus Δ/H at El 58 of Pile 9. 2002-2006

K_h factor development

The data collected from the sensors located at pile 3 and pile 9 were used to produce the maximum K_h factor for each year, shown in Table 4. For the calculations, a constant soil density of 125pcf was used.

Table 4 Maximum K_h factor for every year

Year	K_h value				
	Pile 3		Pile 9		Average
	El 56.5 m	El 58.0 m	El 56.5 m	El 58.0 m	
First	1.6	2.6	1.5	2.3	2.0
Second	2.3	3.3	3.0	3.7	3.0
Third	4.5	4.1	4.2	4.0	4.2
Fourth	4.2	5.5	4.0	3.5	4.3

The change of the coefficient of earth pressure during the first four years of the bridge lifetime is shown in Figure 69. For the first three year, the K_h values (and pressure) increase rapidly, and they reach an upper value by the fourth year.

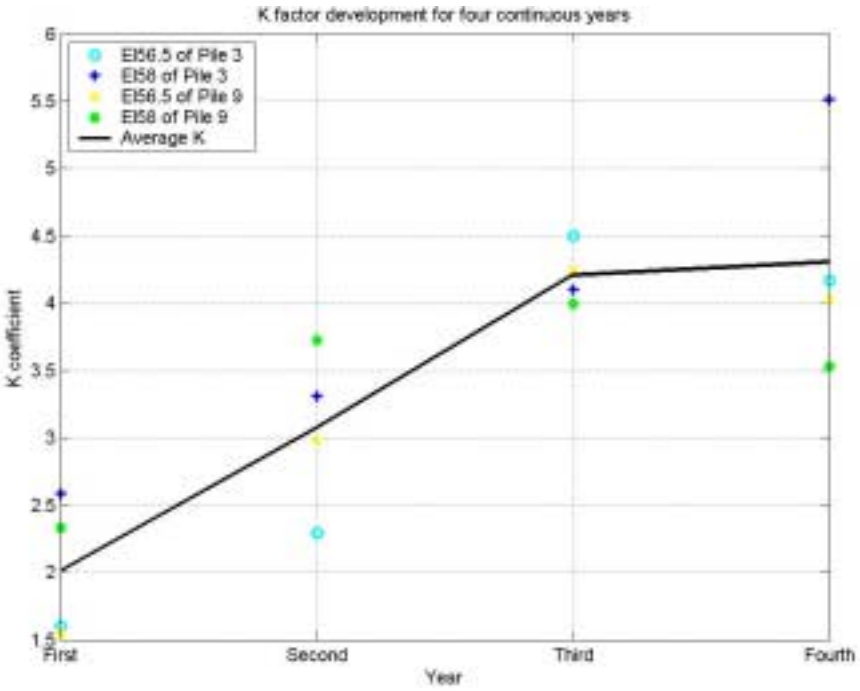

Figure 69. Development of K_h factor over four years

Comparison of the Scotch Road data with other field data

A review of full-scale testing funded by Massachusetts is given in Chapter 4. The Scotch Road data is overlaid with the Massachusetts data in Figure 70 and Figure 71, after adjustments for depth of-measurement and relative time of pressure built up. The data seems to correlate quite well.

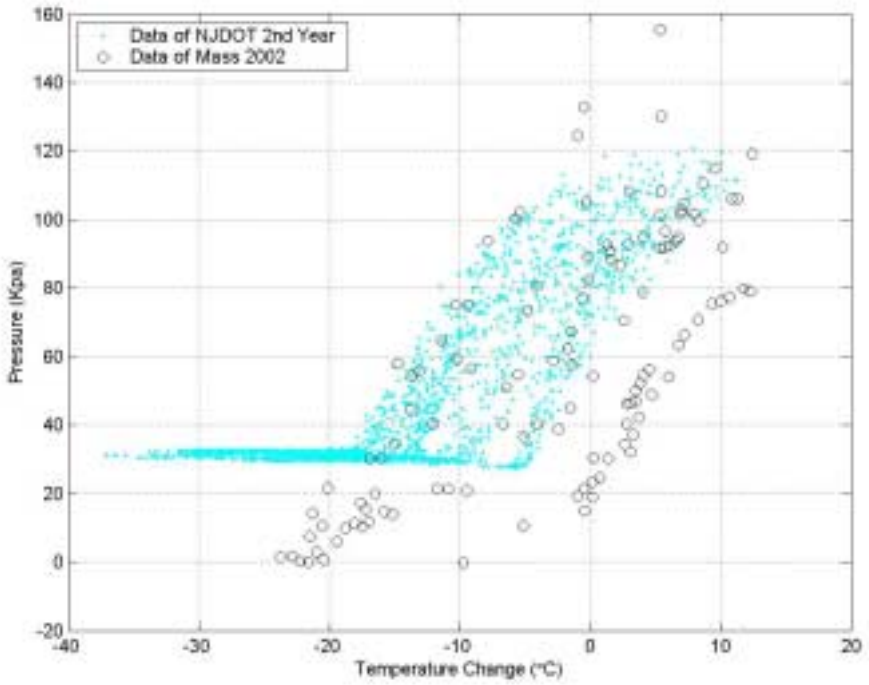

Figure 70. Comparison of average pressure recorded by NJDOT and Massachusetts Highway Department in 2002

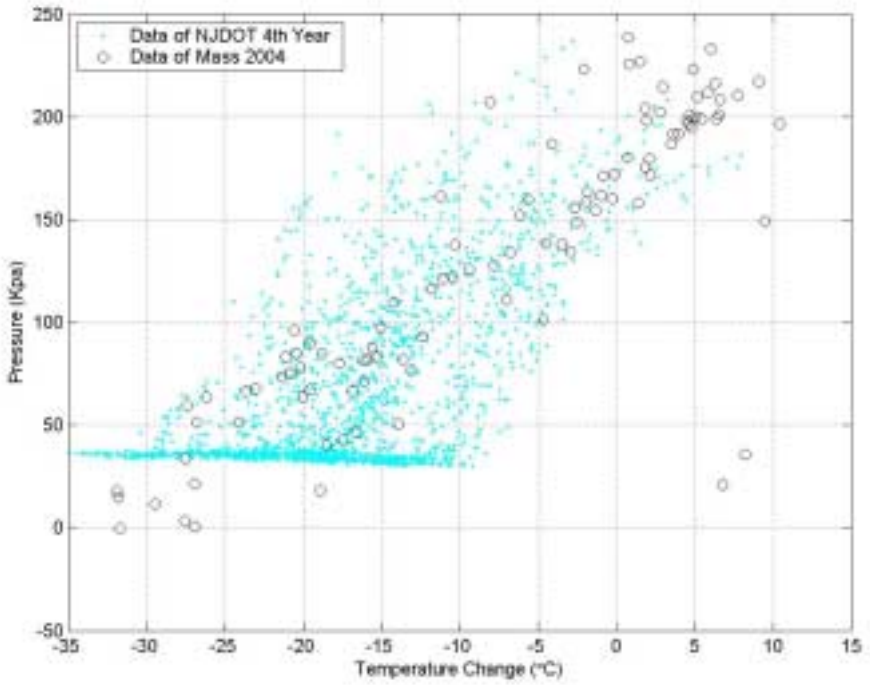

Figure 71. Comparison of average pressure recorded by NJDOT and Massachusetts Highway Department in 2004

Comparison of the recorded data with classic theories

The question of interest is what is the maximum pressure that we should be using to design the abutment. The Scotch Road Bridge was built assuming a Rankine passive pressure of a soil with an angle of internal friction of 30^o. The pressure that has been measured already exceeds the design pressure. But the data and design values are closer if we can assume that the angle of internal friction increased to 40^o due to the densification. To show, the data has been plotted along the depth of the abutment in Figure 72 and is compared to Rankine, Caquot and Kerisel (1948), Shields and Tolunay (1973). [10,31] For the calculations, the height of the abutment is 11 ft (3.35m), the soil density 125pcf, and the angle of internal friction 40^o. The wall is assumed frictionless, and the soil perfectly drained. The passive pressure coefficients are tabulated in Table 5 for several angles of internal friction. The maximum value for Δ/H that was achieved at the abutment is approximately 0.007, however, we assume that

this displacement was large enough to guarantee that the classical methods are applicable. (Such values are shown in Table 1.)

The data shows that an array of the theories can be used to approximate the pressure behind the abutment, for a Φ of 40 and a δ of 0.

Table 5- Classical Passive Pressure Coefficients

Φ	δ	K_p Rankine/ Coulomb	K_p Caquot/ Kerisel	K_p Shields/ Tolunay
30	0	3.0	3.0	3.0
	25	7.7	5.7	4.64
35	0	3.69	3.5	3.69
	25	11.0	8.0	6.21
40	**0**	**4.60**	**4.4**	**4.69**
	25	16.5	11.	8.51
45	0	5.83	5.9	5.83
	25	26.7	19.	12.04

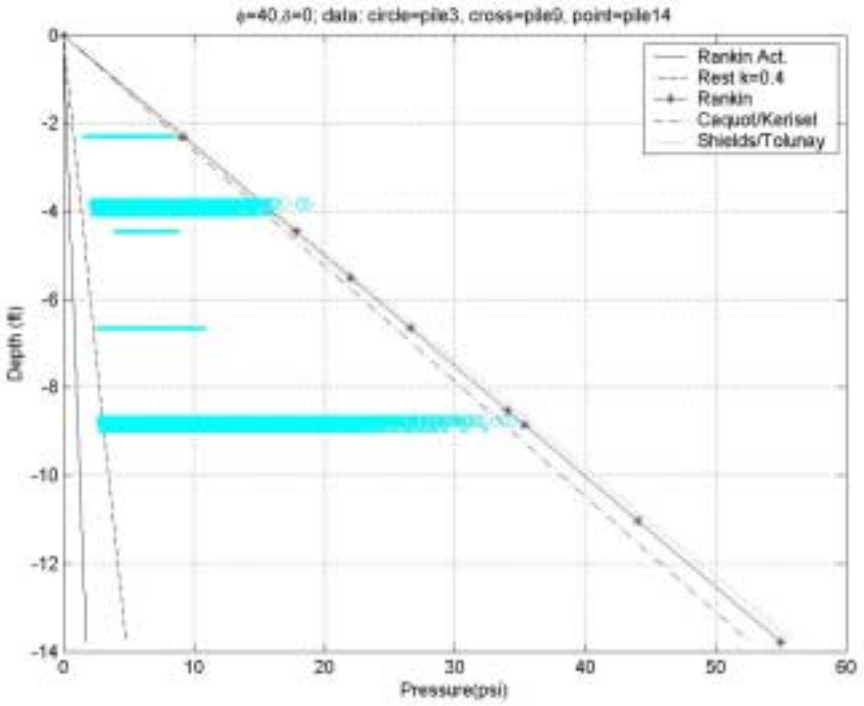

Figure 72. Comparison of data with classical passive pressures 2002-2006

Comparison of the recorded data with displacement-dependent theories

In Figure 73, the data is plotted against the more recent theories that predict passive pressure as a function of abutment rotation for Δ/H of 0.007. The coefficients for these methods are tabulated in Table 6. The British code (BA42), and [19] underestimate the pressures at the base of the abutment. This is mainly due to the fact that the assumption used is of pure rotation and in the pile-supported abutment of the Scotch Road Bridge the motion was mainly translation. The NCHRP proposed K_h factor seems to predict the pressure very well.

Table 6- Passive Pressure Coefficients Dependent on wall-top displacement

Δ/H	K_p Mass Higway[1]	K_p NCHRP for dense sand[1]	K_h BA 42 Code[2] K_p=12.5	K_h England et al. (2000)[2] K_p=12.5
0.001	1.42	2.01	4.17	2.02
0.002	2.23	3.48	4.17	2.86
0.004	3.46	5.04	4.55	4.13
0.006	4.31	5.57	5.35	5.16
0.007	4.62	5.72	5.69	5.62
0.010	5.27	5.80	N/A	N/A
0.020	6.00	5.80	N/A	N/A
0.040	6.12	5.80	N/A	N/A

[1] Triangular pressure distribution along wall

[2] Triangular pressure down to H/2; constant thereafter.

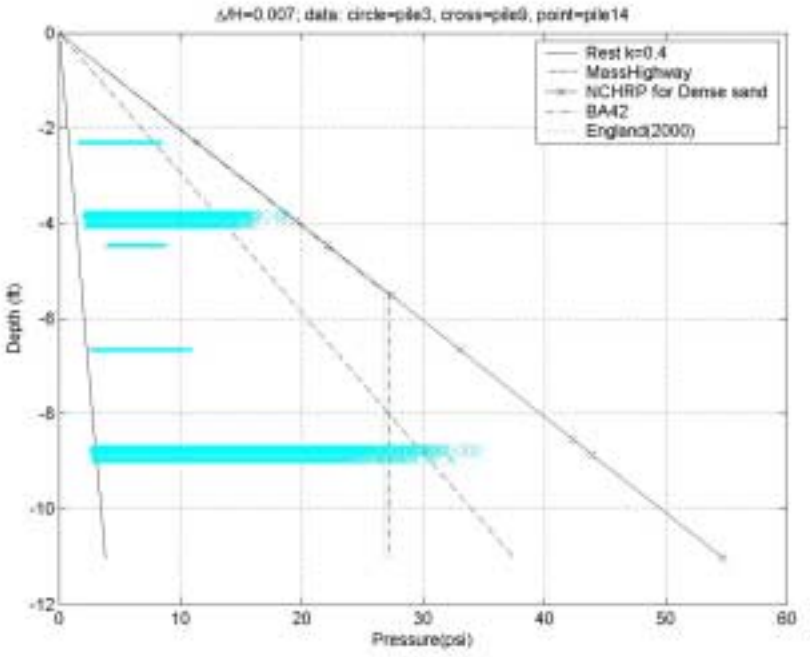

Figure 73. Comparison of data with methods specifically developed to calculate passive pressure behind integral abutments Δ/H=0.007 (2002-2006)

CHAPTER 7-SUMMARY AND CONCLUSIONS

The full-scale testing of the Scotch Road integral abutment and other tests reported in the literature demonstrate that:

1. Integral abutments experience both translation and rotation induced by the daily and seasonally temperature variation. The rotation is relatively small compared with the translation.
2. The total displacement of the integral abutment is a linear function of the temperature variation.
3. The soil behind the abutment experiences pressure build-up due to the densification of the granular soil as a result of the daily and seasonal active and passive cycles for the first three years. Such changes slow down by the fourth year.
4. For relatively small displacements of the bridge, a passive earth pressure coefficient K_h can be taken from the NCHRP proposed K curve for dense sands.
5. The K_h coefficient does not increase with the increasing displacement of the bridge. Rather it decreases a little as the bridge overcomes the original resistance of the soil. The maximum K_p factor recorded didn't exceed the NCHRP proposed K_p factor for dense sand.
6. The earth pressure distribution along the integral abutment seems to be linear. However, only two sensors were used, and data very close to the point of rotation at the top of the piles was not recorded.

Based on the observation above, we conclude that the pressure development behind an integral abutment can be considered to be a function of the soil properties and the displacement of the abutment. In classical calculations, an increase of density will inevitably produce an increase in the pressure. It is also well documented that granular soils flow and rearrange their fabric during cyclic loading leading to an increase of density and thus pressure.

For a relatively short bridge, which experiences small abutment displacements, the classic theories overestimate the passive pressure because a small

displacement will produce pressures between passive and at-rest. In these cases, the NCHRP proposed K_p value for dense sand should be used.

For bridges that are long enough to produce displacements that guarantee the applicability of the classical theories, the NCHRP seems to be overly conservative and overestimates the passive pressure coefficient. Instead, a Rankine Passive K_p value can be used. K_p should be calculated with a maximum internal friction angle for the soil, to simulate the densification due to the cyclic loading . The stress distribution along the abutment for both cases can be taken as triangular, as shown in Appendix A.

Although a maximum pressure should be used in the design of the abutment, it should be noted that this is not the case when designing the superstructure itself. For some load combinations, the bending moments induced by lateral earth pressures on abutments counteract the bending moments due to the dead and live load on the superstructure. The NYSDOT does not recommend using lateral earth pressure in the calculation of midspan moments.

APPENDIX A: Earth Pressure calculation example

For an integral abutment bridge, with cohesionlesss backfill.

Given that: L = the length of the continuous bridge;

H = the depth of the Abutment;

α= the coefficient of thermal expansion;

ΔT = the Annual temperature difference;

γ = the density of the backfill;

ϕ *= the back fill's internal friction angle;*

Solution:

For translational deformation mode, the pressure distribution along the abutment is linear (see Figure 74):

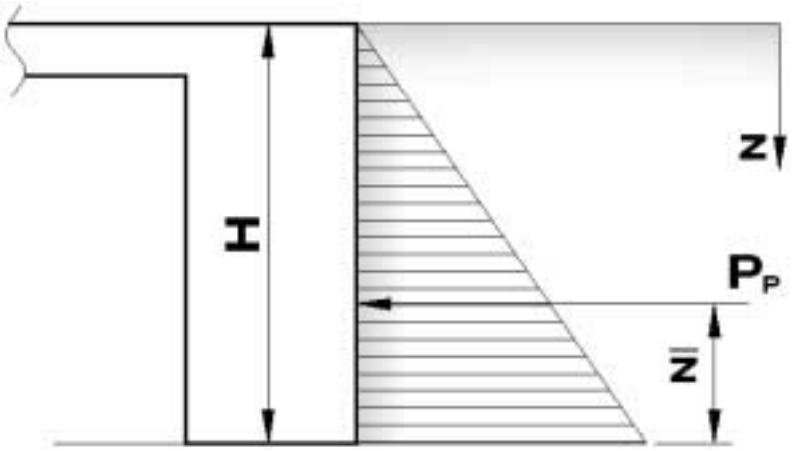

Figure 74. Pressure distribution for translational deformation

The annual maximum displacement of the bridge Δ is:

$$\Delta = \frac{1}{2} L \alpha \Delta T$$

So, we can write the relative wall displacement as:

$$\Delta / H = \frac{L \alpha \Delta T}{2H}$$

According the conclusion we made before, the K_p factor to be used is:

$$K_p = \begin{cases} \text{Rankine passive with an increased } \phi & \text{(for long bridge)} \\ \text{NCHRP curve for dense sand} & \text{(for short bridge)} \end{cases}$$

So the maximum pressure is:

$$\sigma_p = K_p \sigma_o = K_p \gamma z$$

The pressure distribution diagram is shown in Figure 74. The passive force per unit length of the wall is:

$$P_p = \frac{1}{2} \sigma_p H$$

$$= \frac{1}{2} K_p \gamma H^2$$

Also:

$$\bar{z} = \frac{H}{3}$$

REFERENCES

[1] Gabriela Tlustochowicz “Optimized Design of Integral Abutments for a Three Span Composite Bridge” MS Thesis, Lulea University of Technology

[2] John S. Horvath. (2000). “Integral-Abutment Bridges: Problems and innovative Solutions Using EPS Geofoam and Other Geosynthetics” *Manhattan College Research Report No. CE/GE-00-2*

[3] Alberta DOT, Canada,“Guidelines for Design of Integral Abutments”

[4] Arsoy, S., Barker, R.M., and Duncan, J.M. The Behavior of Integral Abutment Bridges. VTRC 00-CR3. Virginia Transportation Research Council 1999; Charlottesville, Va.

[5] Hassiotis, S. and Roman, E. (2005) “A survey of current issues on the use of integral abutment bridges.” Journal of Bridges structures, vol 1,No.2, June 2005, pp81-101.

[6] Oesterle, R. G., Refai, T. M., Volz, J. S., Scanlon, A., and Weiss, W. J. (1998) “Jointless and integral abutment bridges analytical research and proposed design procedures.” *Rep. No. DTFH61-92-C-00154*, Federal Highway Administration, United States Department of Transportation, Washington, D.C.

[7] Kunin, J. and Alampalli, S. (2000) “Integral abutment bridges: Current Practice in United States and Canada.” Journal of Performance of Constructed Facilities, Vol. 14, No. 3. Auguest, 104-111.

[8] Wasserman, E.P.(2001). Design of Integral Abutments for Jointless Bridges. *Structure Magazine*, May, 24-33.

[9] Morgenstern, N. R., and Eisenstein, Z. (1970). "Methods of estimating lateral loads and deformations." *Proc., ASCE Speciality Conf. on Lateral Stresses in the Ground and Design of Earth-Retaining Structures*, Ithaca, N.Y., 51–102.

[10] Caquot, A., and Kerisel, J (1948). Tables for the calculation of passive pressure, active pressure, and bearing capacity of foundations. Gauthier-Villars, Paris.

[11] Brinch-Hansen, J. (1953). *Earth pressure calculation*, Danish Technical Press, Copenhagen, Denmark.

[12] Janbu, N. (1957). "Earth pressure and bearing capacity calculations by generalized procedure of slices." *Proc., 4th Int. Conf. on Soil Mechanics and Foundations Engineering, London, 207–212.*

[13] Sokolovski, V. V. (1960). *Statics of soil media*, Butterworths, London.

[14] Terzaghi, K. and Peck, R. B. (1967). *Soil mechanics in engineering practice,* 2nd Ed., Wiley, New York.

[15] Broms, B. B. and Ingleson, I. (1971). "Earth pressure against the abutments of a rigid frame bridge." *Géotechnique*, Institue of Civil Engineeing., U.K., 21 (1), 15-28.

[16]Bang, S. (1984). "Active Earth Pressure behind Retaining Walls." *Technical note, Journal of Geotechnical Engineering*, ASCE, 111(3), March, 407-412.

[17] Clough, G. W. and Duncan, J. M. (1991). "Earth Pressures, Chapter in Foundation Engineering Handbook." 2nd edition, edited by Hsai-Yang Fang, van Nostrand Reinhold, New York, NY, 223-235.

[18] Chang, Ming-Fang. (1997). "Lateral Earth Pressures Behind Rotating Walls." Canadian Geotechnical Journal, Vol. 34, August, 498-509.

[19] England G. L, David B. I., Tsang, N. C. M. (2000). "Integral Bridges: A Fundamental Approach to the Time-Temperature Loading Problem." London: Telford.

[20] Chen, Yohchia. (1997). "*Important considerations, guidelines, and practical details of integral bridges"*, Journal of Engineering Technology, Vol. 14, Spring 1997, pp. 16-19.

[21] Burke Jr., M.P. (1993). "*The design of integral concrete bridges"*, Concrete International, Vol. 15, June, pp. 37-42.

[22] Das, B.M. (2002) Principles of Geotechnical Engineering, Brooks/Cole Fifth Edition.

[23] J. Michael Duncan, Robert L. Mokwa,(2001) "Passive earth pressure: Theories and tests" *Journal of Geotechnical and Geoenvironmental Engineering, Vol. 127, No. 3, March, 2001.*

[24] Chu, S.-C., and Su, J. J. (1994). ''A method for passive pressure earth computation on sands.'' *Proc., 8th Int. Conf. on Methods and Adv. in Geomechanics*, Siriwardane and Zaman, eds., Vol. 3, Balkema, Rotterdam, The Netherlands, 2441–2445.

[25] Kumar, J., and Subga Rao, K. S. (1997). ''Passive pressure coefficients, critical failure surface and its kinematic admissibility.'' *Geotechnique*, London, 47(1), 185–192.

[26] Soubra, A. H. (2000). ''Static and seismic earth pressure coefficients on rigid retaining structures.'' *Can. Geotech. J.*, Ottawa, 37, 463–478.

[27] Zhu, D.-Y., and Qian, Q. (2000). ‘‘Determination of passive earth pressure coefficients by the method of triangular slices.’’ *Can. Geotech. J*., Ottawa, 37, 485–491.

[28] Robert L. Mokwa, “Investigation of the Resistance of Pile Caps to Lateral Loading” Dissertation of PhD, Virginia Polytechnic Institute and State University Appendix F.

[29] Theodore A. Thomson, Jr. “Passive earth pressures behind integral bridge abutments” Dissertation of Doctor of Philosophy, University of Massachusetts Amherst , 1999

[30] Bishop A.W., “The Use of the Slip Circle in the Stability Analysis of Slopes”, *Geotechnique*, Vol.5, No.1, 1955, pp.7-17

[31] Shields, D.H. and Tolunay, A.Z. (1973). “Passive pressure coefficients by method of slices,” Journal of the Soil Mechanics and Foundations Division, ASCE, Vol 99, No. SM12, 1043-1053.

[32] Khodair, Y.A. and Hassiotis, S. (2005) “Analysis of soil-pile interaction in integral abutment.” Computers and Geotechnics, 32, 201-209.

[33] Massachusetts Bridge Manual, Part I, December 1999

[34] Yung-Show Fang, Tsang-Jiang Chen, and Bin-Ferng Wu. (1994) “Passive earth pressures with various wall movements” *Journal of Geotechnical Engineering, Vol. 120, No. 8, August, 1994.*

[35] Neil C. M. Tsang, George L. England, Treve Dunstan (2002) “Soil/structure interaction of integral bridge with full height abutments” *15th ASCE Engineering Mechanics Conference June 2-5, 2002, Columbia University, New York, NY*

[36] Bonczar, C., Breña, S.F., Civjan, S.A., DeJong, J., Crellin, B., and Crovo, D. “Field Data and FEM Modeling of the Orange-Wendell Bridge”, Proceedings: 2005 FHWA Conference: Integral Abutment and Jointless Bridges (IAJB 2005), Baltimore, MD, 17-19 March 2005, pp163-173.

[37] Scott A. Civjan, Christine Bonczar, Sergio F. Brena, Jason DeJong, and Daniel Crovo. “Integral Abutment Bridge Behavior: Parametric Analysis of a Massachusetts Bridge” *Journal of Bridge Engineering, Vol. 12, No. 1, January 1, 2007.*

[38] Kongsak Pugasap. (2006) “Hysteresis model based prediction of integral abutment bridge behavior” Dissertation for Doctor of Philosophy, The Pennsylvania State University

[39] Khodair, Y. A. (2004) “Numerical and Experimental Analysis of an Integral Abutment Bridge”, Ph.D. Dissertation, Stevens Institute of Technology, Hoboken, N.J.

[40] Sensing Systems and Associates (2002). New Bedford, Mass.

[41]Hassiotis,* S. (2003) “The Scotch-Road Bridge Project”, 5th Annual NJDOT Showcase, Rutgers University, October 24.

[42] Hassiotis,* S, Lopez, J.A. and Bermudez, R. (2005) “Full-Scale Testing of an Integral Abutment Bridge.” Proceedings, FHWA Integral Abutment and Jointless Bridges IAJB 2005. Baltimore, Maryland, March 16-18, pp. 199-210

[43] National Cooperative Highway Research Program (NCHRP). (1991). “Manuals for the design of bridge foundations.” R. M. Barker, J. M.Duncan, K. B. Rojiani, P. S. K. Ooi, C. K. Tan, and S. G. Kim, eds., *Transportation Research Record. 343*, Transportation Research Board, Washington, D.C.

[44] Syed Abdul Mofiz, Mohd. Raihan Taha, and Dipopk Chandra Sharker, (2004) “Mechanical stress-strain characteristics and model behaviour of geosynthetic reinforces soil composites” *17th ASCE Engineering Mechanics Conference June 13-16, 2004, University of Delaware, Newark, DE*

[44] Greimann, L.F., Wolde-Tinsae, A.M., and Yang, P. S. (1983). “Skewed Bridges with Integral Abutments.” Transportation Research Record, n. 903, 99. 64-72.